Culvert Rehabilitation using 3D Printed Diffusers

Final Report
June 2024

Principal Investigator:
Roberto Lopez-Anido
Advanced Structures and
Composites Center

University of Maine

Authors
Roberto Lopez-Anido
Sunil Bhandari

Sponsored By
Transportation Infrastructure Durability Center
List other Sponsors if applicable (i.e. MaineDOT)

A report from
University of Maine
Transportation Infrastructure
and Durability Center
https://tidc.umaine.edu/

About the Transportation Infrastructure Durability Center

The Transportation Infrastructure Durability Center (TIDC) is the 2018 US DOT Region 1 (New England) University Transportation Center (UTC) located at the University of Maine Advanced Structures and Composites Center. TIDC's research focuses on efforts to improve the durability and extend the life of transportation infrastructure in New England and beyond through an integrated collaboration of universities, state DOTs, and industry. The TIDC is comprised of six New England universities, the University of Maine (lead), the University of Connecticut, the University of Massachusetts Lowell, the University of Rhode Island, the University of Vermont, and Western New England University.

U.S. Department of Transportation (US DOT) Disclaimer

Acknowledgements

Funding for this research is provided by the Transportation Infrastructure Durability Center at the University of Maine under grant 69A3551847101 from the U.S. Department of Transportation's University Transportation Centers Program. [Include any acknowledgements for other contributors (i.e. your university or contributing DOTs/industry partners) here.]

Technical Report Documentation Page

1. Report No.	**2. Government Accession No.**	**3. Recipient Catalog No.**
4 Title and Subtitle Culvert Rehabilitation using 3D Printed Diffusers		**5 Report Date** June 2024 **6 Performing Organization Code**
7. Author(s) Roberto Lopez-Anido https://orcid.org/0000-0001-8702-0642 Sunil Bhandari https://orcid.org/0000-0002-2748-3095		**8 Performing Organization Report No.**
9 Performing Organization Name and Address University of Maine 168 College Ave Orono, Maine 04469		**10 Work Unit No. (TRAIS)** **11 Contract or Grant No.**
12 Sponsoring Agency Name and Address		**13 Type of Report and Period Covered** Final Report (dates of project) **14 Sponsoring Agency Code** 69A3551847101
15 Supplementary Notes		

16 Abstract

Due to the increasing number of deteriorating and failing culverts under highways in Maine and across the nation, efforts have been underway to reduce costs by slip lining selected culverts rather than replacing them. While slip lining extends the useful life of culverts, it reduces the diameter of both the culvert and the inlet thus reducing culvert capacity. Utilizing diffuser technology can more than compensate from the reduction in capacity that results from the slip lining process. This trenchless technology of slip lining a culvert and adding a performance enhancing diffuser outlet can extend the useful life of the culvert by decades without compromising capacity. A partnership between MaineDOT and UMaine has provided a unique opportunity to utilize large-scale 3D printing technology to design and manufacture diffusers with the specific geometry required for each field installation. Whereas the use of fiberglass or reinforced concrete would require different forms for each different size diffuser, 3D printing can simply add a scaling factor to an existing diffuser design. Large-scale 3D printing technology using low-cost materials shows great promise in designing and manufacturing inexpensive and site-specific diffusers. Because the addition of a diffuser would eliminate the reduced capacity resulting from slip lining, this cost-effective trenchless technology could be used much more broadly.

17 Key Words Culvert Diffusers Additive Manufacturing		**18 Distribution Statement** No restrictions. This document is available to the public through	
19 Security Classification (of this report) Unclassified	**20 Security Classification (of this page)** Unclassified	**21 No. of pages**	**22 Price**

Form DOT F 1700.7 (8-72)

Composites Part C: Open Access 18 (2025) 100659

Contents lists available at ScienceDirect

Composites Part C: Open Access

journal homepage: www.sciencedirect.com/journal/composites-part-c-open-access

Durability of large-format additively manufactured polymer composite structures with environmental exposure–accelerated water immersion

Sunil Bhandari [a,b,*], Prabhat Khanal [a,b], Roberto A. Lopez-Anido [a,b]

[a] Department of Civil and Environmental Engineering, University of Maine, Orono, ME 04469, USA
[b] Advanced Structures and Composites Center, University of Maine, Orono, ME 04469, USA

ARTICLE INFO

Keywords:
LFAM
Additive manufacturing
Durability
Moisture
Accelerated ageing

ABSTRACT

Large-format additive manufacturing (LFAM) of polymer composites enables rapid production of large-scale components for infrastructure, transportation, and defense. As these components see increased outdoor use, understanding their durability under moisture exposure is critical. This study evaluates the effects of water immersion on the durability of LFAM composites using three material systems: carbon fiber reinforced acrylonitrile butadiene styrene (CF-ABS), glass fiber reinforced polyethylene terephthalate glycol (GF-PETG), and wood flour reinforced amorphous polylactic acid (WF-aPLA). Specimens were fabricated using a pellet-fed extrusion-based LFAM process and immersed in water for 30, 60, and 90 days at three temperatures. Moisture uptake and mechanical degradation were assessed in both longitudinal and through-thickness orientations to capture the influence of interlayer interfaces. Results show that bio-based WF-aPLA absorbed significantly more moisture than petroleum-based CF-ABS and GF-PETG and exhibited ongoing degradation that prevented saturation. The most severe mechanical losses occurred in the through-thickness direction, where more interbead interfaces and voids were present. Longitudinal specimens showed better retention of strength and stiffness. Mechanical property degradation progressed in two stages: an initial rapid phase following an Arrhenius relationship with inverse temperature, and a slower secondary phase that deviated from this behavior. The findings demonstrate that both material selection and build orientation significantly affect moisture durability. While petroleum-based composites performed better overall, their durability remains influenced by LFAM-induced anisotropy. These results support material selection and predictive modeling for reliable LFAM structures in outdoor environments.

Introduction

Polymer composite parts produced using large-format additive manufacturing (LFAM) have been used in exterior environment applications. The broadening of additive manufacturing (AM) technology to encompass larger-scale capabilities promises to transform numerous industries by providing more efficient, cost-effective, and adaptable manufacturing solutions [1]. In polymer extrusion-based AM, LFAM is generally designated as an AM process capable of producing parts that are considerably larger than typical desktop-scale printers, with higher deposition rates and larger-diameter extruded beads. Nieto and Molina [2] describe LFAM as a 3D printing technology capable of build volumes over one cubic meter. The study for polymer extrusion-based 3D printing highlights the use of pellet-based extrusion systems in LFAM in contrast to filament-based extrusion systems in desktop-scale 3D printers and mentions that the extruded beads in LFAM systems have diameters larger than 2.5 mm. Similarly, Vicente et al. [3] describe LFAM as systems capable of producing parts larger than 1 cubic meter and further classify LFAM into medium-sized AM (MSAM) and high-size AM (HSAM). Machines with build volumes between one and seven cubic meters are identified as MSAM, and machines with build volumes greater than seven cubic meters are identified as HSAM.

Polymer extrusion-based LFAM has found applications in several industries. Najmon et al. [4] described several applications of LFAM in the aerospace industry. Chambon et al. [5] presented the use of LFAM for the development of the vehicle powertrain of a utility vehicle. Jafferson et al. [6] demonstrated design and manufacturing of airless tires using LFAM of thermoplastic polyurethane (TPU). Ziółkowski and Dyl [7] reviewed the applications of LFAM technologies in the shipbuilding industry. Transportation infrastructures like culvert outlet diffusers [8] and formwork for precast concrete structures [9] have been manufactured using LFAM of polymer composites.

* Corresponding author.
E-mail address: sunil.bhandari@maine.edu (S. Bhandari).

https://doi.org/10.1016/j.jcomc.2025.100659

Available online 9 October 2025

Several thermoplastic composites have been used as feedstock materials for LFAM. Love [10] reported on the rapid manufacturing of customized electric vehicles with carbon fiber reinforced acrylonitrile butadiene styrene (CF-ABS) composites using big area additive manufacturing (BAAM), which was one of the first LFAM equipment. Duty et al. studied the structure and mechanical behavior of CF-ABS parts manufactured using LFAM [11]. The research work concluded that the addition of reinforcing fibers can improve stiffness and strength but introduces a high degree of anisotropy. Ajineru et al. [12] studied the rheological behavior of carbon fiber (CF) reinforced polymers, polyphenylsulphone (CF-PPS), polyethylsulphone (CF-PES), polyphenylene sulphide (CF-PPS), and CF-ABS. The extrusion screw speed and temperature were identified as the process parameters that can be varied to manufacture complex geometry parts. Post et al. [13] studied the economic viability of using several polymer composites for the LFAM process to manufacture composite tooling. The study evaluated polyether ether ketone (PEEK), ULTEM, PPS, PPSF, and PPFSU polymers for the economic viability of LFAM molds and found significant savings in terms of time and money compared to conventionally manufactured molds. Bhandari et al. [8] used bio-based wood flour reinforced polylactic acid (WF-PLA) to manufacture prototype-culvert outlet diffusers for rehabilitation of deteriorated culverts. Lopez-Anido et al. [14] used LFAM CF-ABS to manufacture formworks used for casting precast concrete structures in railroad bridge rehabilitation.

The durability of thermoplastic composites for applications that involve environmental exposure has been well studied. Stark et al. [15] studied the durability of wood fiber-reinforced high-density polyethylene and found that the composite materials decreased in mechanical performance and were more susceptible to biological attacks when exposed to a high-moisture environment. Pomies and Carlson [16] studied the durability of glass fiber-reinforced polyphenylene sulfide when subjected to moisture exposure and proposed a numerical model to predict the reduction in mechanical properties of the composite. Zhou et al. [17] compared the performance difference between thermoplastic polypropylene and thermosetting epoxy, both reinforced with carbon fiber, when subjected to elevated temperatures, water immersion, and sustained bending loading. The study found that polypropylene composites exhibited better environmental durability compared to epoxy composites. Zhao et al. [18] studied the hygrothermal aging behavior and mechanical degradation of ramie/carbon fiber reinforced hybrid thermoplastic composites and found that moisture diffusion across cross-section is faster than on the surface. Ghazebi et al. [19] studied the long-term effects of saltwater ageing on 3D printed polyamide-6 reinforced with carbon fiber, Kevlar fiber, and glass fiber. The study found that increasing fiber volume fraction increases water absorption and that the flexural strength of 3D printed composites.

Some research works that study the durability of polymer composites that were 3D printed on a desktop scale show the degradation in mechanical properties of the 3D printed parts. Banjo et al. [20] studied the moisture-induced changes in the mechanical properties of 3D printed nylon, carbon fiber-reinforced nylon, and PLA. The study found significant property degradation in the studied polymer composite systems, with flexural modulus of nylon decreasing by as much as 60 percent after degradation. The study highlighted the plasticization and hydrolytic cleavage due to moisture absorption as the reason for the reduction in mechanical properties. However, the effect of layerwise manufacturing and the voids was not studied. Elmushyakhi [21] studied the effects of freeze-thaw exposure of 3D printed polyetherimide and found that freeze-thaw conditioning reduced the mechanical properties of the 3D printed parts. Microscopic computed tomography showed an increase in void volume, cracking, and distortion in the extruded cross-section in the specimens subjected to freeze-thaw cycling. Pizzorni and Prato [22] studied the effects of hygrothermal aging on the tensile and bonding performance of 3D printed carbon fiber reinforced polyamide-6. The 3D printed composites were consolidated by pressing and used as substrates of structural epoxy-adhesive joints. The study showed that post-printing consolidation is beneficial as it causes a reduction in void volume fraction that partially counteracts moisture absorption.

For large-format additive manufacturing, the voids due to the layered deposition of extruded material introduce more voids and wider interfaces. Duty et al. [11] found bubbles within deposited beads and voids between the extruded beads. The contact area is 30 to 50 % between the beads in the same layer and 70 % between the beads in adjacent layers. Such continuous voids make the LFAM parts more susceptible to moisture ingress. Saavedra-Rojas et al. [23] studied the flexural properties of WF-PLA and CF-ABS parts manufactured using LFAM. The results showed that the bio-based polymer composites were more susceptible to degradation caused by moisture, which resulted in significantly lower mechanical properties.

While there are several studies on the durability of conventionally manufactured polymer composites, and a few on desktop-scale 3D printed composites, the durability of Large-format additively manufactured (LFAM) polymer composites under environmental exposure remains largely unexplored. Moreover, it is unknown whether the degradation mechanisms observed in LFAM are the same as in conventional composites, particularly given the unique anisotropy, void distribution, and interlayer interfaces inherent to LFAM processes. This study aims to systematically investigate accelerated water immersion of LFAM composites across petroleum-based and bio-based systems, comparing both longitudinal and through-thickness orientations to isolate the role of interlayer interfaces. By combining physical, thermal, and mechanical testing with predictive modeling, the work provides novel insights into degradation mechanisms specific to LFAM composites, filling a key gap in durability assessment for their use in infrastructure and outdoor applications. The objectives of this study are:

1. Study the durability of LFAM polymer composites exposed to moisture.
2. Characterize the loss in mechanical properties of LFAM polymer composites with an increase in exposure to the external environment.
3. Model and predict the degradation of LFAM polymer composite parts to guide the design of load-bearing components.

Materials and methods

Materials

Three thermoplastic polymer composites were used for this study:

1. CF-ABS (Carbon Fiber–reinforced Acrylonitrile Butadiene Styrene), specifically LNP™ THERMOCOMP™ AM AC004XXAR1 from SABIC, is a compounded thermoplastic material containing 20 % of chopped carbon fiber by weight within a conventional petroleum-based ABS matrix. This material is widely used in polymer LFAM due to its favorable balance of printability, stiffness, dimensional stability, and mechanical strength. Its prevalence in industrial LFAM applications makes it a benchmark for evaluating long-term durability under mechanical loading and thermal cycling. Studying CF-ABS provides valuable insights into the performance boundaries of traditional, non-biodegradable thermoplastic composites in demanding service environments.
2. GF-PETG (Glass Fiber–reinforced Polyethylene Terephthalate Glycol), marketed as HiFill® PETG 1701 3DP by Techmer PM, is a thermoplastic composite containing 20 % of glass fiber by weight. Compared to unfilled PETG, the inclusion of glass fibers enhances toughness, impact resistance, and creep performance, while also improving chemical resistance and environmental stability. These properties make GF-PETG a strong candidate for durability studies, particularly in applications exposed to moisture or outdoor conditions.

3. WF-aPLA (Wood Fiber–reinforced amorphous Polylactic Acid), sold as Jabil PLA 3120 WF, is a bio-based thermoplastic composite containing 20 % wood fiber by weight. This material represents a more sustainable alternative to petroleum-based composites and is typically used in aesthetic or low-load-bearing applications. Its inclusion in this study enables the assessment of how natural fiber–reinforced and potentially biodegradable materials degrade over time, in comparison to conventional engineered thermoplastics.

Methods

Sample preparation

A Tradesman Series P3-44 3D printer from JuggerBot3D was used to manufacture the specimens. The 3D printer has a heated vacuum bed and a heated, insulated printing chamber. The print envelope is 1168 mm in X, 889 mm in Y, and 939 mm in Z. Two nozzles were available for this machine: a 4 mm diameter nozzle and a 10 mm diameter nozzle. Typically, bead geometry for the ø4 mm nozzle is 6 mm wide by 1.5 mm tall. For the ø10 mm nozzle, the typically used bead geometry is 15 mm wide by 3.75 mm tall. For this study, a 10 mm nozzle was used to create a bead geometry with a width of 15 mm and a height of 3.75 mm. A total of two beads per layer was used to manufacture the hollow hexagonal prisms. Table 1 shows the printing parameters used for additive manufacturing of the polymer composite specimens used in this study.

Fig. 1 shows the process of manufacturing the test specimens used for the durability studies. Hollow hexagonal prisms were manufactured using the JuggerBot3D LFAM equipment. The hexagonal prisms were cut into six walls. Each wall was placed on a waterjet cutting equipment and test specimens were cut out. Test specimens were cut from the walls with two length orientations: specimen type-X (length aligned with the direction of the deposition of extruded polymer) and specimen type-Z (length aligned with the direction of the stacked layers).

The dimensions of all the specimens used for tensile testing were 200 mm long, 30 mm wide, and 7.5 mm thick. The gauge region of the central 50 mm length of the specimen was monitored during the test. The grip lengths were 25 mm on both sides. The dimensions of the specimens were in accordance with the ASTM D3039 [24] for tensile testing. Fig. 2 shows the GF-PETG and type-X and type-Z specimens used for the study. The type-X specimens have two visible interfaces along the length of the specimen. The type-Z specimens have 54 interfaces along the length of the specimen.

Evaluation of physical properties

Polymer molecular weight. Measurements of changes in molecular weight of polymers after accelerated water ageing was performed to evaluate polymer degradation and understand mechanical property loss. Polymer molecular weight was determined experimentally by gel permeation chromatography (GPC). The experiment used an Agilent 1260 Infinity Size Exclusion Chromatography system with a temperature-controlled refractive index array. The method followed was similar to that of Khoda et al. [25] Schweizer et al. [26] also followed a similar method to determine the polymer molecular weight of 3D-printed CF-ABS and WF-aPLA. The method required the dissolution of the polymer in a solvent. Samples weighing approximately 5 mg were dissolved in high-performance liquid chromatography (HPLC) grade tetrahydrofuran, which served as the solvent. The polymer concentration ranged from 1 mg/mL to 3 mg/mL. Before injection, samples were filtered through a 0.2 µm PTFE syringe filter. The analysis used tetrahydrofuran as the eluent at a 1 mL/min flow rate. The tests were conducted at a temperature of 35 °C.

GPC was used to measure the molecular weight of the compounded material's baseline and water-immersed specimens. The tests were done for the X-specimens as shown in Fig. 2. The specimens were immersed in water at 40 °C for 90 days. The tests were performed to evaluate whether accelerated water immersion causes chain scission of the polymers used in this study.

Table 1
Printing parameters for WF-aPLA, GF-PETG, and CF-ABS.

Parameter	WF-aPLA	GF-PETG	CF-ABS
Extrusion temperature (°C)	200	215	245
Bed temperature (°C)	50	60	95
Layer time (min:*sec*)	3:38	3:23	2:43
Deposition travel speed (mm/min)	850	808	1148
Layer height (mm)	3.75	3.75	3.75
Aspect ratio of layer (bead width/bead height)	4.00	4.00	4.00
Deposition rate (kg/hr)	3.50	4.50	4.40

Measurement of specific gravity. Previous research works showed that reduction in mechanical properties of 3D printed polymer composites after accelerated water immersion ageing [18,23,27]. In this research work, the "specific gravity" of the composites was measured for different temperature and time conditioning to check if there was a change in specific gravity that corresponds to change in mechanical properties. A decrease in specific gravity suggests material degradation or formation of voids. The specific gravity of specimens was measured following Test Method A of ASTM D792, which includes testing solid plastics in water. The mass of the specimen in air was measured. The specimen was immersed in water, and its apparent mass upon immersion was determined to calculate the specific gravity of the specimen. Three specimens were used to calculate an average value for the specific gravity of each set of material and conditioning. The specific gravity of the specimen was calculated using Eq. (1).

$$SG = a/(a + w - b) \tag{1}$$

where,

a = apparent mass of the specimen, without wire, in air,
b= apparent mass of the specimen completely immersed and of the wire partially immersed in liquid, and
w= apparent mass of partially immersed wire.
The change in specific gravity was used to determine if the accelerated water immersion tests introduced voids into the 3D printed polymer composite specimens.

Thermal property characterization

Change in glass transition temperature has been used by researchers to identify the effects of ageing and degradation of polymer [28,29]. Glass transition temperature was measured for the polymer composites to identify conditioning temperature since the conditioning temperatures had to be chosen below glass transition temperature. Furthermore, the glass transition temperature was measured to check if water immersion accelerated ageing affects the glass transition temperature of 3D printed thermoplastic specimens. Glass transition temperature was evaluated experimentally using Differential Scanning Calorimetry (DSC). DSC tests were conducted in accordance with ASTM E1356. Colón Quintana et al. [30] and Schweizer et al. [26] followed a similar procedure to measure glass transition temperature in their study. The samples were analyzed using a TA Instruments DSC2500 (TA Instruments, New Castle, DE, USA) in TA Tzero Aluminum pans. The DSC process involved the following steps:

1. Equilibrate at 20 °C
2. Ramp 10 °C /min to 200 °C (First Heating)
3. Isothermal for 1 min
4. Ramp 10 °C /min to 20 °C (Cooling)
5. Isothermal for 1 min
6. Ramp 10 °C /min to 200 °C (Second Heating)

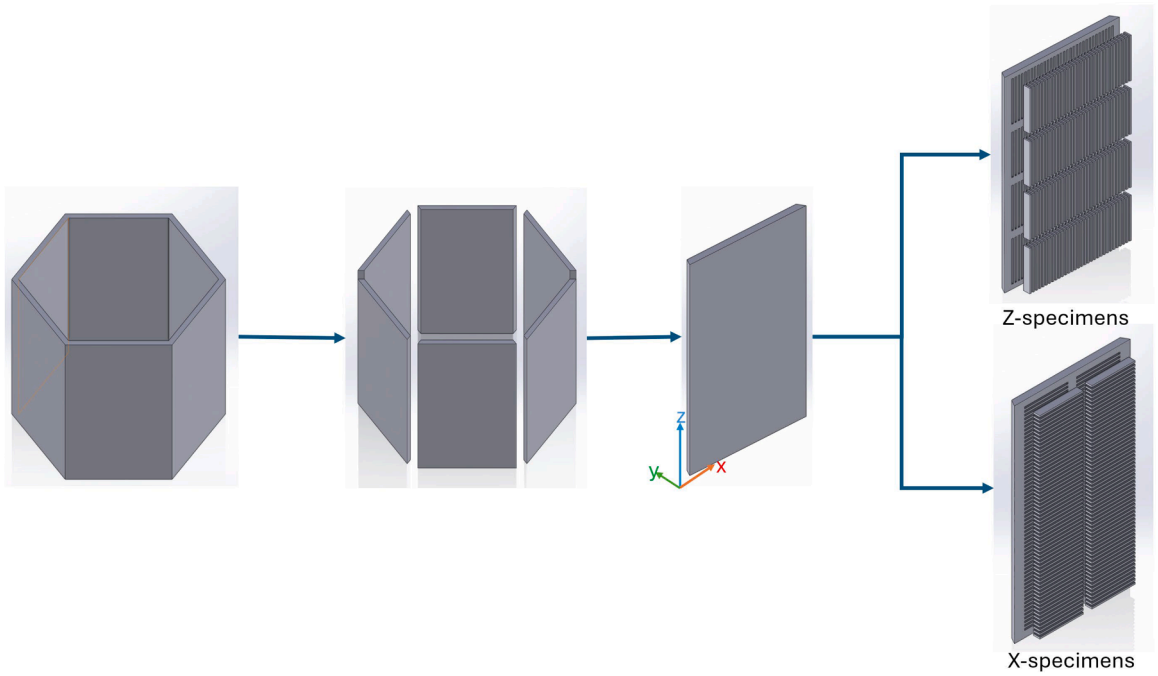

Fig. 1. Process of manufacturing test specimens for the durability study.

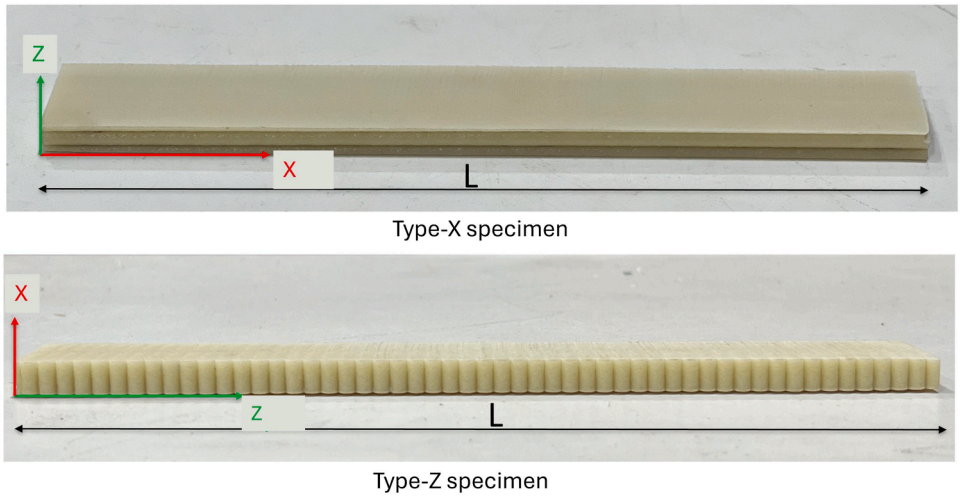

Fig. 2. Type-X and type-Z-specimens of GF-PETG material used for the study.

The initial heating step provides the thermal properties resulting from the manufacturing process. The cooling step was an annealing process to homogenize the material and achieve equilibrium. The second heating step reveals the actual properties of the material [30]. The sample, weighing between 4 and 10 mg, was placed in a pan and covered with a lid. Another empty pan was taken, closed with a lid, and weighed. Both masses were then input into the program, and the program was run. The glass transition temperature (Tg) was determined from the heat flow curves generated during the second heating ramps. The results were analyzed using TA Universal Analysis software. The midpoint temperature was taken as the glass transition temperature, as defined by ASTM E1356. The average of three samples was taken as the mean Tg.

Accelerated water immersion

An accelerated water immersion methodology was employed to study the longevity of the LFAM polymer composite parts. ASTM D5229 [31] test standard was adopted for the study. This test method describes a procedure for determining moisture absorption or desorption properties in the through-the-thickness direction for single-phase Fickian solid materials in flat or curved panels. The dimensions of specimens subjected to accelerated water immersion were 200 mm long, 30 mm wide, and 7.5 mm thick. The same specimens were used for tension tests to evaluate the loss in mechanical properties after accelerated ageing. The specimens were immersed in distilled water procured from Chem-World. The elevated temperature for oven-dry and accelerated water immersion was selected based on the conditioned materials' glass transition temperature (Tg). A related study on material characterization using Differential Scanning Calorimetry (DSC) provided the Tg for three composite materials: 1) CF-ABS, Tg= 106.8 °C; 2) GF-PETG, Tg= 76.1 °C; and WF-aPLA, Tg= 54.8 °C. Hence, the temperature of 40 °C (below the Tg of all materials) was selected. Each set of specimens was dried in an oven at 40 °C until the change in mass of the specimen was less than 1%. The dried specimens were immersed in distilled water for 90 days at 40 °C. The specimens were weighed at 48 or 72 h intervals,

depending on the lab schedule. The specimens were taken out of the distilled water bath and wiped off with an absorbent cloth. The weight of the specimen was measured using a OHAUS AX4202/E precision balance with precision of 0.01 g.

A 90-day maximum time was chosen for water immersion. The choice was based on literature review and practicability. Many prior studies used 90 days as a benchmark, making it easier to compare results across different research. The 90-day maximum time was considered as a reasonable compromise so that it is long enough to observe significant degradation trends without overextending into impractically long experiments. Moisture content was calculated, and sorption curves were generated following ASTM D5229 from the set of specimens immersed for 90 days. The sets of specimens were subjected to accelerated water immersion at the elevated temperature of 40 °C for either 30, 60, or 90 days, followed by tensile testing.

Later, the same procedure was followed for two more temperatures: 55 °C and 70 °C for CF-ABS and GF-PETG and 23 °C and 30 °C for WF-aPLA. Table 2 shows the conditioning temperatures for different polymer composite materials.

Average moisture content (M) was calculated using Eq. (2).

$$M = \frac{W_i - W_o}{W_0} * 100\% \tag{2}$$

where:

W_i = current specimen mass, and
W_o = oven-dry specimen mass.

Mechanical property characterization using ASTM tension tests

The tensile test was performed on a 100 KN servo-hydraulic load frame from Instron, equipped with hydraulic grips. Tests were conducted at the environmentally controlled Material Testing Lab (MTL) at the Advanced Structures and Composites Center at the University of Maine. The lab temperature was 21.0 °C to 25.0 °C (69.8°F - 77.0°F), and the relative humidity was 40 % - 60 %. WaveMatrix2 Software was used to create and run a test method to test materials with the frame. The method included testing the specimens at a standard head displacement rate of 2 mm/min, according to ASTM D3039. For each timestamp, the applied force and position of the crosshead were recorded for the entire duration of testing.

The strains were recorded using non-contact digital image correlation. A 3D-Digital Image Correlation (DIC) system from GOM ARAMIS, Germany, was used to record full-field strains over an area of 50 mm along the axial direction and 30 mm in the transverse direction on the test specimen surface during the testing. The specimens were spray-painted to create a stochastic black and white pattern in the gage region of the specimens. This allowed full-field strain measurement to be recorded during the entire duration of testing. The strain data was recorded at a frequency of 1 Hz. Using GOM correlate, mean axial strain and mean transverse strain were obtained for the entire duration of testing. Further, the ultimate tensile strain was recorded as the maximum strain before failure in the longitudinal or axial direction.

Modeling reduction in mechanical properties

Accelerated aging techniques are based on the empirical principle that chemical reactions, including those causing material deterioration, follow the Arrhenius reaction rate function [32,33] According to this function, generally, a 10 °C increase in the temperature of a homogeneous process leads to a doubling of the chemical reaction rate [33]. The Arrhenius model is commonly applied when temperature is the primary factor in accelerating aging. It operates under the assumption that a single dominant degradation mechanism remains constant throughout the exposure period, while the degradation rate increases with higher exposure temperatures [34]. The Arrhenius relation is given by Eq. (3).

$$K(T) = A.e^{-\frac{Ea}{RT}} \tag{3}$$

where,

K is a reaction rate or degradation rate
A is a constant
Ea is the process activation energy
R is the universal gas constant
T is the absolute temperature

The Arrhenius relationship is extensively used to predict the lifespan of polymers and composites by evaluating their ultimate mechanical properties and retention, such as tensile strength, interfacial shear strength, creep strength, and fatigue strength [35–37]. In polymeric matrix composites, it is assumed that temperatures close to the glass transition temperature (Tg) are not used. Under these conditions, the tensile strength retention (SR) of GFRP composite laminates, which is the ratio of residual strength to original tensile strength, is determined from experimental data for each exposure temperature (T). These data points are plotted against the logarithm of time, enabling predictions of strength loss over longer periods and varying temperatures. According to the method used by Davalos et al. [38], it is assumed that the percentage of strength retention during accelerated aging tests, SR, can be expressed as Eq. (4), where t is the time of exposure.

$$\mathrm{SR} = \mathrm{SR(t)} = 100 * e^{-kt} \tag{4}$$

This expression implies a total loss of strength if time t reaches the limit. Plotting the experimental values of stress retention against the corresponding aging times enables the determination of the degradation rate k through regression analysis, valid if the correlation coefficient is above 0.8 [39]. The time required to reach a specified tensile strength retention at a different temperature can be calculated using Eq. (4). All temperature regression curves should have approximately equal slopes; otherwise, the degradation mechanism is dependent on temperature [40].

In many studies, the durability prediction approach relies on the time shift concept [38,40–42]. Dejke [42] utilized the time shift factor (TSF) concept, defined as the ratio of the times needed for a specific reduction in a mechanical property at two different temperatures. The time required for a reaction is inversely proportional to the reaction rate k. Therefore, the ratio of t1, the time needed for a specific property reduction at temperature T1, to t2, the time required for the same reduction at temperature T2, can be expressed as Eq. (5) [35].

$$TSF = \frac{t2}{t1} = \frac{Ae^{-\frac{Ea}{RT2}}}{Ae^{-\frac{Ea}{RT1}}} = e^{\frac{Ea}{R}\left(\frac{1}{T1}-\frac{1}{T2}\right)} \tag{5}$$

The time shift factor (TSF) enables the estimation of degradation under actual service conditions using data from accelerated aging experiments [43]. It involves adjusting the laboratory data (e.g., strength retention) along the time axis to determine the time t1 at which the same level of degradation is projected to occur at a lower temperature. Once the TSF is obtained from experimental data, the activation energy (Ea/R) can be calculated, allowing the use of regression curves to predict strength retention under field conditions and a specified time [40].

Table 2
Conditioning temperatures for different polymer composite materials.

Material	Conditioning temperatures (°C)		
	T1	T2	T3
CF-ABS	40	55	70
GF-PETG	40	55	70
WF-aPLA	23	30	40

Results and discussion

Accelerated water immersion ageing results

Physical properties

Changes in molecular weight. Table 3 presents the GPC results for molecular weights of polymers under study for baseline and accelerated water-immersed specimens.

The results show 4.0 %, 20 %, and 64 % reduction in mean molecular weight and 3.3 %, 16 %, and 69 % increase in polydispersity for CF-ABS, GF-PETG, and WF-aPLA, respectively, after water immersion at 40 °C for 90 days. The results indicate the degradation of all three polymers (ABS, PETG, and aPLA) after water immersion at 40 °C. The degradation in bio-based aPLA is the highest among the three. Further, the polydispersity was found to increase, resulting in a broader molecular weight distribution. The broadness of molecular weights was higher in the case of bio-based aPLA compared to petroleum-based polymers.

Changes in specific gravity. Table 4 summarizes the results for the average specific gravity of baseline and 90-day accelerated water-immersed specimens for petroleum-based materials (CF-ABS and GF-PETG) and bio-based material (WF-aPLA) respectively. The average was taken from the specific gravity of three specimens for every condition. The values in parenthesis represent the coefficient of variation (cv).

The results show a less than 1 % change in the specific gravity of petroleum-based materials (CF-ABS and GF-PETG) after accelerated water immersion at elevated temperatures. For bio-based WF-aPLA, the specific gravity after accelerated water immersion at 40 °C was reduced by 6.5 % for both type-X and type-Z specimens.

Changes in glass transition temperature. Table 5 shows the glass transition temperatures of the polymer composites used for the study before and after the accelerated water immersion test. The baseline mean Tg for CF-ABS, GF-PETG, and WF-aPLA were found to be 106.8 °C, 76.1 °C, and 54.8 °C, respectively. The values obtained are comparable to the available literature. Schweizer et al. [26] reported the Tg values of 102 °C for CF-ABS and 54.4 °C for WF-aPLA. Similarly, Bin et al. [44] reported Tg for CF-ABS to be approximately 100 °C. Colón Quintana et al. [30] reported the Tg of 104–108 °C for CF-ABS and 77–78 °C for GF-PETG. No significant change in glass transition temperature was found after accelerated water immersion.

Water absorption. Table 6 presents the average moisture content after water immersion at three different temperatures for 90 days for all three materials.

In the case of CF-ABS, the water content of 1.6 % in specimens X and 1.3 % in specimens type-Z was observed after water immersion at 40 °C for 90 days. Saavedra-Rojas et al. [9] observed similar results for CF-ABS with a water content of 1.35 % after water immersion at 40 °C for 81 days.

It was found that bio-based WF-aPLA has the highest water content of 10.1 % in specimens type-Z after exposure at 40 °C for 90 days compared to petroleum-based materials. Saavedra-Rojas et al. [23] observed similar results for WF-aPLA with a water content of 9.23 % after water immersion at 40 °C for 81 days.

WF-aPLA specimens did not reach their saturation point. CF-ABS specimens subjected to water immersion at 55 °C and 70 °C reached

Table 4
Specific gravity of composite after 90 days of water immersion.

Material	Specimen type	Baseline	Water immersion temperature				
			23 °C	30 °C	40 °C	55 °C	70 °C
CF-ABS	X	1.10 (0.7 %)	-	-	1.11 (0.2 %)	1.10 (0.3 %)	1.11 (0.5 %)
	Z	1.09 (0.2 %)	-	-	1.10 (1.1 %)	1.10 (1.2 %)	1.11 (0.5 %)
GF-PETG	X	1.33 (0.4 %)	-	-	1.33 (0.7 %)	1.33 (0.3 %)	1.32 (0.4 %)
	Z	1.33 (0.3 %)	-	-	1.32 (0.5 %)	1.33 (0.3 %)	1.32 (0.6 %)
WF-aPLA	X	1.24 (1.1 %)	1.22 (0.5 %)	1.18 (0.2 %)	1.15 (1.0 %)	-	-
	Z	1.22 (0.2 %)	1.22 (0.4 %)	1.22 (0.3 %)	1.14 (0.6 %)	-	-

Table 5
Glass transition temperatures of polymer composites subjected to accelerated water immersion.

Composite	Conditioning	Mean glass transition temperature (°C)
CF-ABS	Baseline	106.8 (0.1)
	30 days	107.3 (0.1)
	60 days	107.0 (0.2)
	90 days	107.3 (0.1)
GF-PETG	Baseline	76.1 (0.1)
	30 days	76.5 (1.1)
	60 days	76.2 (0.0)
	90 days	75.9 (0.4)
WF-aPLA	Baseline	54.8 (0.0)
	30 days	54.7 (0.2)
	60 days	54.4 (0.1)
	90 days	54.6 (0.1)

Table 6
Moisture content in specimens subjected to accelerated water immersion.

Material	Specimen type	Moisture content (%)				
		23 °C	30 °C	40 °C	55 °C	70 °C
CF-ABS	**X**	-	-	1.6	1.6	1.6
	Z	-	-	1.3	1.4	1.5
GF-PETG	**X**	-	-	1.3	1.4	2.1
	Z	-	-	1.0	1.2	2.1
WF-aPLA	**X**	3.8	5.9	8.2	-	-
	Z	4.5	6.6	10.1	-	-

Table 3
The effect of accelerated water immersion on the molecular weight of polymers.

Material	Mean molecular weight- baseline	Average peak molecular weight - baseline	Mean molecular weight- water immersion	Average peak molecular weight - water immersion	PD - baseline	PD - water immersion
CF-ABS	60.8	154	58.4	153	2.09	2.16
GF-PETG	17.9	52.8	14.3	50.6	2.53	2.94
WF-aPLA	83.2	187	30.1	138	2.04	3.45

saturation point. GF-PETG specimens subjected to water immersion at 55 °C reached their saturation point.

Based on the effective moisture equilibrium criteria as per ASTM D5229, the specimens can be considered to have reached moisture equilibrium if the average moisture content of the specimens changes by less than 0.020 % over each of two consecutive reference time spans. At 40 °C, none of the specimens reached moisture equilibrium (saturation point). The changes in moisture content of CF-ABS and GF-PETG were relatively small and the rates of water absorption were getting slower. At 55 °C, equilibrium was reached for CF-ABS and GF-PETG. At 70 °C, equilibrium was reached for CF-ABS. However, GF-PETG continued to absorb water at a significant rate even after 90 days. Even though this temperature is below the glass transition temperature of PETG (76.1 °C), it is very close. Similar results have been reported by other researchers for water absorption of polymers at temperatures close to glass transition temperature. At all temperatures (23 °C, 30 °C, and 40 °C) the changes in moisture content of WF-aPLA was significantly large and the rate of water absorption did not slow down. Similar results have been reported in published research work regarding water absorption of WF-aPLA composites.

Fig. 3 shows the sorption curves for the polymer composite specimens.

Change in mechanical properties. Tables 7 and 8 show the mechanical properties of CF-ABS type-X and type-Z specimens subjected to accelerated water immersion. The results for CF-ABS type-X specimens show that after 90 days of water immersion, the average tensile strength is reduced by 10 %, 25 %, and 36 % at 40 °C, 55 °C, and 70 °C, respectively. However, the average tensile modulus is relatively unaffected (<5 % reduction).

The results for CF-ABS in the through-thickness direction indicate that after 90 days of water immersion, average tensile strength is reduced by 5.8 %, 32 %, and 32 % at 40 °C, 55 °C, and 70 °C,

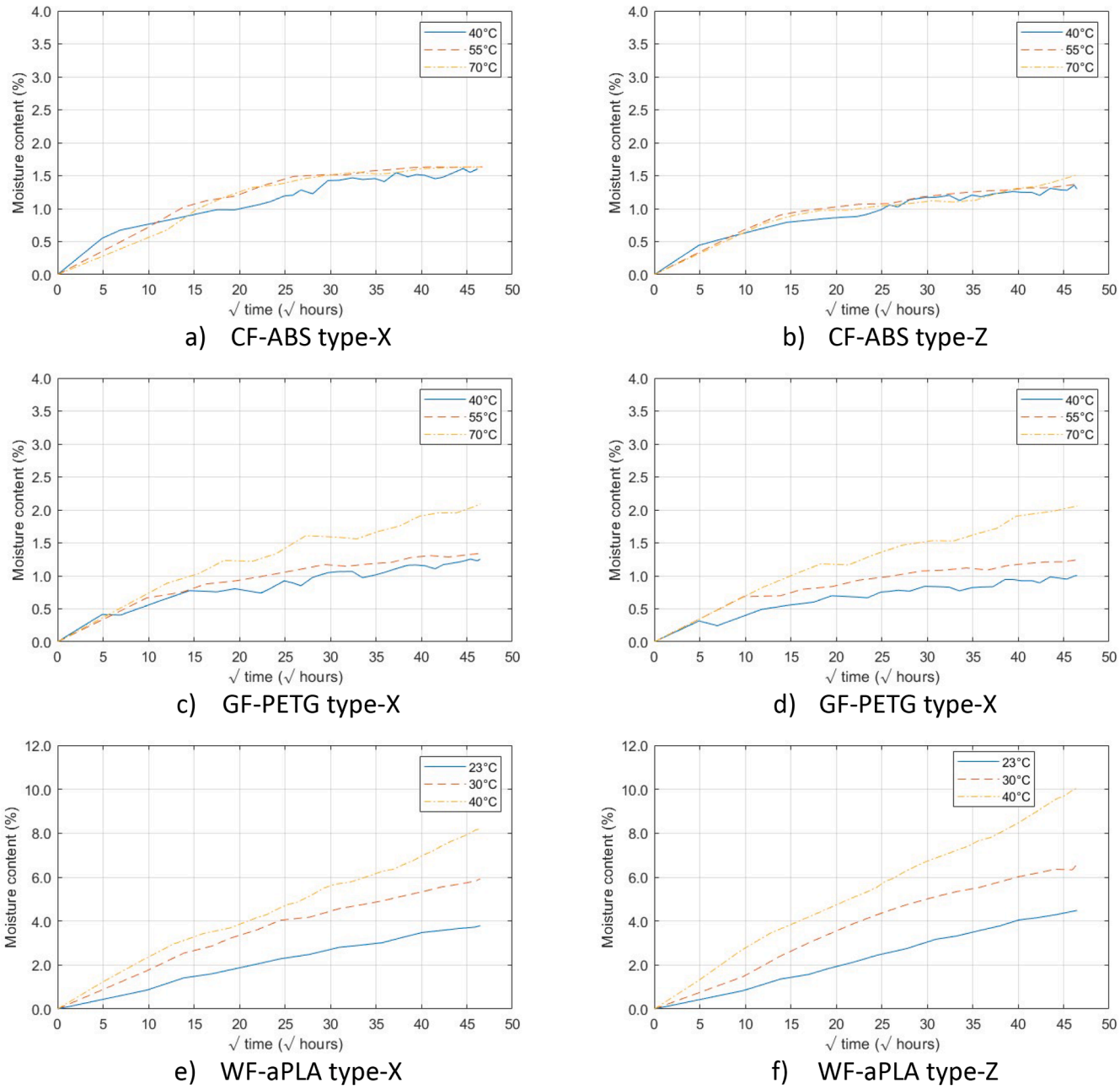

Fig. 3. Sorption curves of polymer-composite specimens.

Table 7
Mechanical properties of CF-ABS type-X specimens subjected to accelerated water immersion.

Exposure	F (MPa)	E (GPa)	Strain to failure (%)	Poisson's ratio
Baseline	75.4 (3.3 %)	11.3 (2.8 %)	0.80 (6.7 %)	0.39 (5.4 %)
Water/ 40 °C/30 days	70.5 (14 %)	11.4 (3.5 %)	0.75 (15 %)	0.39 (14 %)
Water/ 40 °C/60 days	66.2 (13 %)	11.7 (4.9 %)	0.63 (21 %)	0.41 (17 %)
Water/ 40 °C/90 days	67.8 (9.5 %)	11.5 (4.7 %)	0.66 (15 %)	0.42 (14 %)
Water/ 55 °C/30 days	62.1 (5.6 %)	11.4 (3.6 %)	0.60 (8.6 %)	0.39 (4.4 %)
Water/ 55 °C/60 days	56.2 (6.4 %)	11.4 (1.5 %)	0.53 (8.0 %)	0.39 (4.2 %)
Water/ 55 °C/90 days	56.7 (7.3 %)	11.3 (1.8 %)	0.54 (10 %)	0.39 (5.1 %)
Water/ 70 °C/30 days	57.3 (6.3 %)	11.3 (1.1 %)	0.55 (7.7 %)	0.40 (3.6 %)
Water/ 70 °C/60 days	51.1 (7.1 %)	11.1 (1.4 %)	0.49 (9.2 %)	0.40 (6.4 %)
Water/ 70 °C/90 days	48.6 (5.7 %)	10.8 (1.2 %)	0.49 (8.8 %)	0.40 (3.2 %)

Table 8
Mechanical properties of CF-ABS type-Z specimens subjected to accelerated water immersion.

Exposure	F (MPa)	E (GPa)	Strain to failure (%)	Poisson's ratio
Baseline	17.1 (6.8 %)	2.63 (4.9 %)	0.69 (6.1 %)	0.40 (9.8 %)
Water/ 40 °C/30 days	17.0 (3.5 %)	2.63 (3.5 %)	0.68 (3.6 %)	0.37 (4.7 %)
Water/ 40 °C/60 days	16.0 (7.8 %)	2.66 (4.0 %)	0.64 (9.9 %)	0.42 (6.8 %)
Water/ 40 °C/90 days	16.1 (7.6 %)	2.63 (2.0 %)	0.66 (7.8 %)	0.42 (4.8 %)
Water/ 55 °C/30 days	12.4 (9.7 %)	2.67 (1.5 %)	0.48 (11 %)	0.39 (3.4 %)
Water/ 55 °C/60 days	11.3 (7.2 %)	2.59 (1.3 %)	0.45 (7.8 %)	0.38 (4.6 %)
Water/ 55 °C/90 days	11.6 (13 %)	2.60 (1.5 %)	0.46 (16 %)	0.38 (5.6 %)
Water/ 70 °C/30 days	12.2 (6.0 %)	2.61 (3.3 %)	0.49 (8.0 %)	0.40 (4.4 %)
Water/ 70 °C/60 days	11.2 (10 %)	2.56 (1.3 %)	0.45 (13 %)	0.41 (2.2 %)
Water/ 70 °C/90 days	11.7 (3.5 %)	2.46 (1.5 %)	0.53 (6.0 %)	0.38 (8.8 %)

Table 9
Mechanical properties of GF-PETG type-X specimens subjected to accelerated water immersion.

Exposure	F (MPa)	E (GPa)	Strain to failure (%)	Poisson's ratio
Baseline	67.4 (7.3 %)	6.71 (4.6 %)	1.55 (19 %)	0.39 (15 %)
Water/ 40 °C/30 days	67.9 (5.0 %)	6.82 (2.2 %)	1.51 (14 %)	0.40 (3.0 %)
Water/ 40 °C/60 days	68.7 (5.5 %)	6.78(3.4 %)	1.52 (14 %)	0.39 (4.6 %)
Water/ 40 °C/90 days	62.6 (1.4 %)	6.22 (2.5 %)	1.55 (3.1 %)	0.39 (1.9 %)
Water/ 55 °C/30 days	54.1 (3.6 %)	6.12 (3.9 %)	1.21 (7.7 %)	0.39 (3.0 %)
Water/ 55 °C/60 days	52.5 (3.8 %)	6.07 (2.5 %)	1.16 (5.6 %)	0.39 (3.3 %)
Water/ 55 °C/90 days	56.8 (3.4 %)	6.11 (3.9 %)	1.58 (8.0 %)	0.42 (5.4 %)
Water/ 70 °C/30 days	51.2 (4.1 %)	6.10 (1.8 %)	1.15 (10 %)	0.39 (4.6 %)
Water/ 70 °C/60 days	50.1 (3.6 %)	6.10 (2.8 %)	1.07 (8.1 %)	0.38 (6.0 %)
Water/ 70 °C/90 days	67.4 (7.3 %)	6.71 (4.6 %)	1.55 (19 %)	0.39 (15 %)

Table 10
Mechanical properties of GF-PETG type-Z specimens subjected to accelerated water immersion.

Exposure	F (MPa)	E (GPa)	Strain to failure (%)	Poisson's ratio
Baseline	19.3 (7.8 %)	2.22 (4.5 %)	0.99 (7.7 %)	0.45 (3.1 %)
Water/ 40 °C/30 days	18.2 (5.0 %)	2.27 (4.2 %)	0.96 (5.6 %)	0.46 (7.1 %)
Water/ 40 °C/60 days	19.3 (3.8 %)	2.31 (6.0 %)	0.93 (5.6 %)	0.45 (2.4 %)
Water/ 40 °C/90 days	19.2 (3.9 %)	2.28 (3.0 %)	0.95 (5.8 %)	0.47 (9.1 %)
Water/ 55 °C/30 days	18.4 (3.9 %)	2.23 (0.8 %)	1.03 (6.1 %)	0.46 (2.3 %)
Water/ 55 °C/60 days	17.7 (2.4 %)	2.22 (2.4 %)	1.05 (7.1 %)	0.47 (3.0 %)
Water/ 55 °C/90 days	15.7 (7.8 %)	2.09 (4.5 %)	1.01 (6.6 %)	0.47 (6.5 %)
Water/ 70 °C/30 days	12.8 (11 %)	2.04 (14 %)	0.75 (27 %)	0.45 (8.7 %)
Water/ 70 °C/60 days	9.77 (6.6 %)	1.97 (3.3 %)	0.53 (13 %)	0.46 (4.5 %)
Water/ 70 °C/90 days	7.13 (18 %)	1.97 (3.5 %)	0.36 (24 %)	0.43 (4.2 %)

respectively. The average tensile modulus is relatively unaffected at 40 °C and 55 °C and is reduced by 6.5 % at a higher exposure temperature of 70 °C.

Tables 9 and 10 show the mechanical properties of GF-PETG type-X and type-Z specimens subjected to accelerated water immersion.

The results for GF-PETG type-X specimens show that after 90 days of water immersion at 40 °C, the tensile properties are relatively unaffected. At relatively higher temperatures of exposure, 55 °C and 70 °C, the average tensile strength is reduced by 25 % and 29 %, respectively, and the average tensile modulus is reduced by around 8.5 % in both cases.

The results for GF-PETG in the through-thickness direction show that after 90 days of water immersion, tensile properties are unaffected at 40 °C. At 55 °C and 70 °C, the average tensile strength is reduced by 19 % and 63 %, respectively, and the average tensile modulus is reduced by 5.9 % and 11 %, respectively.

Tables 11 and 12 show the mechanical properties of WF-aPLA type-X and type-Z specimens subjected to accelerated water immersion. The results for WF-aPLA type-X specimens show the following:

- Water immersion at 23 °C: The average tensile strength reduced by 14 %, 17 %, and 22 % and the average tensile modulus by 12 %, 14 %, and 19 % in 30, 60, and 90 days, respectively.
- Water immersion at 30 °C: The average tensile strength reduced by 22 %, 31 %, and 36 % and the average tensile modulus by 20 %, 27 %, and 28 % in 30, 60, and 90 days, respectively.
- Water immersion at 40 °C: The average tensile strength reduced by 29 %, 35 %, and 41 % and the average tensile modulus by 26 %, 30 %, and 37 % in 30, 60, and 90 days, respectively.
- The average tensile strains are relatively increased by 15 % to 62 % after water immersion compared to the baseline samples.

The results for WF-aPLA in the through-thickness show the following:

Table 11
Mechanical properties of WF-aPLA type-X specimens subjected to accelerated water immersion.

Exposure	F (MPa)	E (GPa)	Strain to failure (%)	Poisson's ratio
Baseline	40.3 (2.4 %)	4.36 (2.7 %)	1.27 (7.6 %)	0.34 (7.2 %)
Water/ 40 °C/30 days	34.8 (2.5 %)	3.84 (3.0 %)	1.46 (15 %)	0.34 (4.3 %)
Water/ 40 °C/60 days	33.3 (3.9 %)	3.73 (3.1 %)	1.65 (20 %)	0.32 (16 %)
Water/ 40 °C/90 days	31.3 (4.0 %)	3.54 (4.0 %)	1.94 (14 %)	0.34 (4.1 %)
Water/ 55 °C/30 days	31.5 (1.6 %)	3.49 (1.5 %)	1.69 (16 %)	0.35 (4.1 %)
Water/ 55 °C/60 days	27.7 (3.6 %)	3.18 (5.3 %)	2.06 (29 %)	0.34 (8.4 %)
Water/ 55 °C/90 days	25.8 (2.1 %)	3.13 (2.5 %)	1.73 (17 %)	0.34 (5.3 %)
Water/ 70 °C/30 days	28.8 (3.8 %)	3.22 (5.1 %)	1.81 (20 %)	0.37 (17 %)
Water/ 70 °C/60 days	26.2 (3.8 %)	3.07 (4.6 %)	1.74 (17 %)	0.35 (8.8 %)
Water/ 70 °C/90 days	23.8 (5.3 %)	2.73 (5.3 %)	1.68 (28 %)	0.36 (6.8 %)

Table 12
Mechanical properties of WF-aPLA type-Z specimens subjected to accelerated water immersion.

Exposure	F (MPa)	E (GPa)	Strain to failure (%)	Poisson's ratio
Baseline	21.2 (6.3 %)	3.11 (5.8 %)	0.78 (11 %)	0.37 (17 %)
Water/ 40 °C/30 days	17.4 (6.5 %)	2.78 (3.2 %)	0.72 (7.4 %)	0.37 (3.1 %)
Water/ 40 °C/60 days	15.9 (6.4 %)	2.56 (3.2 %)	0.77 (8.8 %)	0.35 (3.6 %)
Water/ 40 °C/90 days	12.8 (16 %)	2.47 (3.8 %)	0.59 (18 %)	0.37 (2.8 %)
Water/ 55 °C/30 days	15.0 (4.2 %)	2.28 (3.4 %)	0.94 (13 %)	0.36 (4.0 %)
Water/ 55 °C/60 days	13.9 (3.6 %)	2.22 (3.6 %)	0.88 (7.9 %)	0.38 (11 %)
Water/ 55 °C/90 days	12.9 (3.0 %)	2.24 (3.3 %)	0.76 (9.0 %)	0.39 (7.4 %)
Water/ 70 °C/30 days	13.9 (2.2 %)	2.11 (7.8 %)	1.16 (18 %)	0.38 (3.0 %)
Water/ 70 °C/60 days	13.4 (2.3 %)	1.98 (4.1 %)	1.09 (19 %)	0.40 (2.2 %)
Water/ 70 °C/90 days	11.6 (3.2 %)	1.88 (2.6 %)	1.12 (9.8 %)	0.40 (3.5 %)

- Water immersion at 23 °C: The average tensile strength reduced by 18 %, 25 %, and 39 % and the average tensile modulus by 11 %, 18 %, and 21 % in 30, 60, and 90 days, respectively.
- Water immersion at 30 °C: The average tensile strength reduced by 29 %, 34 %, and 39 % and the average tensile modulus by 27 %, 29 %, and 28 % in 30, 60, and 90 days, respectively.
- Water immersion at 40 °C: The average tensile strength reduced by 34 %, 37 %, and 45 % and the average tensile modulus by 32 %, 36 %, and 40 % in 30, 60, and 90 days, respectively.
- The tensile strains are relatively increased after water immersion compared to the baseline samples.

Bio-based WF-aPLA is highly susceptible to water immersion and the reduction in average tensile strength and average tensile modulus when compared to baseline is statistically significant at all three temperatures of water immersion (23 °C, 30 °C, and 40 °C). This is true for both directions under consideration.

Petroleum-based CF-ABS and GF-PETG are less susceptible to water immersion compared to bio-based WF-aPLA. In general, the effect at a relatively lower temperature of 40 °C is statistically insignificant. But as the temperature of immersion increases to 55 °C and 70 °C, the effect is significant. In both cases, the significance of the effect in average tensile strength is greater compared to average tensile modulus.

Based on the effective moisture equilibrium criteria as per ASTM D5229, i.e., the average moisture content of the material changes by less than 0.020 % over each of two consecutive reference time spans, none of the thermoplastic composite materials reached moisture equilibrium after 90 days of accelerated water immersion at 40 °C. So, further acceleration was done for both petroleum-based thermoplastic materials by increasing the temperature of the water immersion bath to reach moisture equilibrium in 90 days. CF-ABS specimens type-X reached the equilibrium moisture content of 1.6 % (after 1680 h/70 days) at 55 °C and 1.6 % (after 1752 h/73 days) at 70 °C. CF-ABS specimens type-Z, GF-PETG, and WF-aPLA did not reach the moisture equilibrium. For WF-aPLA, further acceleration is not feasible by increasing the water bath temperature since it needs to be lower than the Tg. Hence, to reach moisture equilibrium, the water immersion should be conducted for more than 90 days.

For petroleum-based CF-ABS and GF-PETG, it is observed that for all the temperatures of water immersion, the moisture absorption in the first 30 days is comparatively higher compared to the moisture absorption after 30 days of immersion. The mean tensile strength reduction correlates with water absorption and the reduction in the first 30 days of water immersion is comparatively higher and is relatively steady after 30 days of water immersion.

Fig. 4 shows the change in strength of the accelerated water immersion specimens over time at different temperatures. The strength decreases with duration of exposure and temperature.

Fig. 5 shows strength vs moisture content of the specimens subjected to accelerated water absorption. It is observed that the strength decreases with increasing water absorption for the specimens. For bio-based WF-aPLA, it is observed that the mean tensile strength correlates with the moisture content for all three temperatures of water immersion. The rate of water absorption was comparatively higher in the first 30 days of water immersion. The reduction in mean tensile strength was higher in the first 30 days of water immersion and the reduction was relatively slower after 30 days.

Bio-based WF-aPLA experienced the highest moisture content after 90 days of accelerated water at 40 °C compared to petroleum-based composite materials. Moisture content for WF-aPLA type-X specimens was 8.2 % and, in the type-Z specimens, 10.1 %.

Fig. 6 shows the tensile strength and tensile modulus vs normalized mean molecular weight of WF-aPLA type-X specimens.

Bio-based WF-aPLA at 40 °C experienced average tensile strength in the type-X specimens, reduced by 41 %, and in the type-Z specimens, reduced by 45 % after 90 days of accelerated water immersion. The average tensile modulus in the type-X specimens is reduced by 37 %, and in the type-Z specimens is reduced by 40 % after 90 days of accelerated water immersion. This reduction can be attributed to the combination of the following:

- 64 % reduction in mean molecular weight (Mn) (for type X specimens), which implies the polymer is degrading,
- 6.5 % reduction in specific gravity (for both type-X and type-Z), which implies the formation of voids due to polymer degradation and
- moisture content of 8.2 % (type-X specimens) and 10.1 % (type-Z specimens).

Modeling reduction in mechanical properties

Based on the experimental results, the rate of degradation is significantly higher in the first 30 days of water immersion compared to the rate of degradation after 30 days. Hence, it is assumed that the degradation of 3D-printed thermoplastic composites does not follow a single degradation mechanism. Jiang et al. [27] observed three stages of

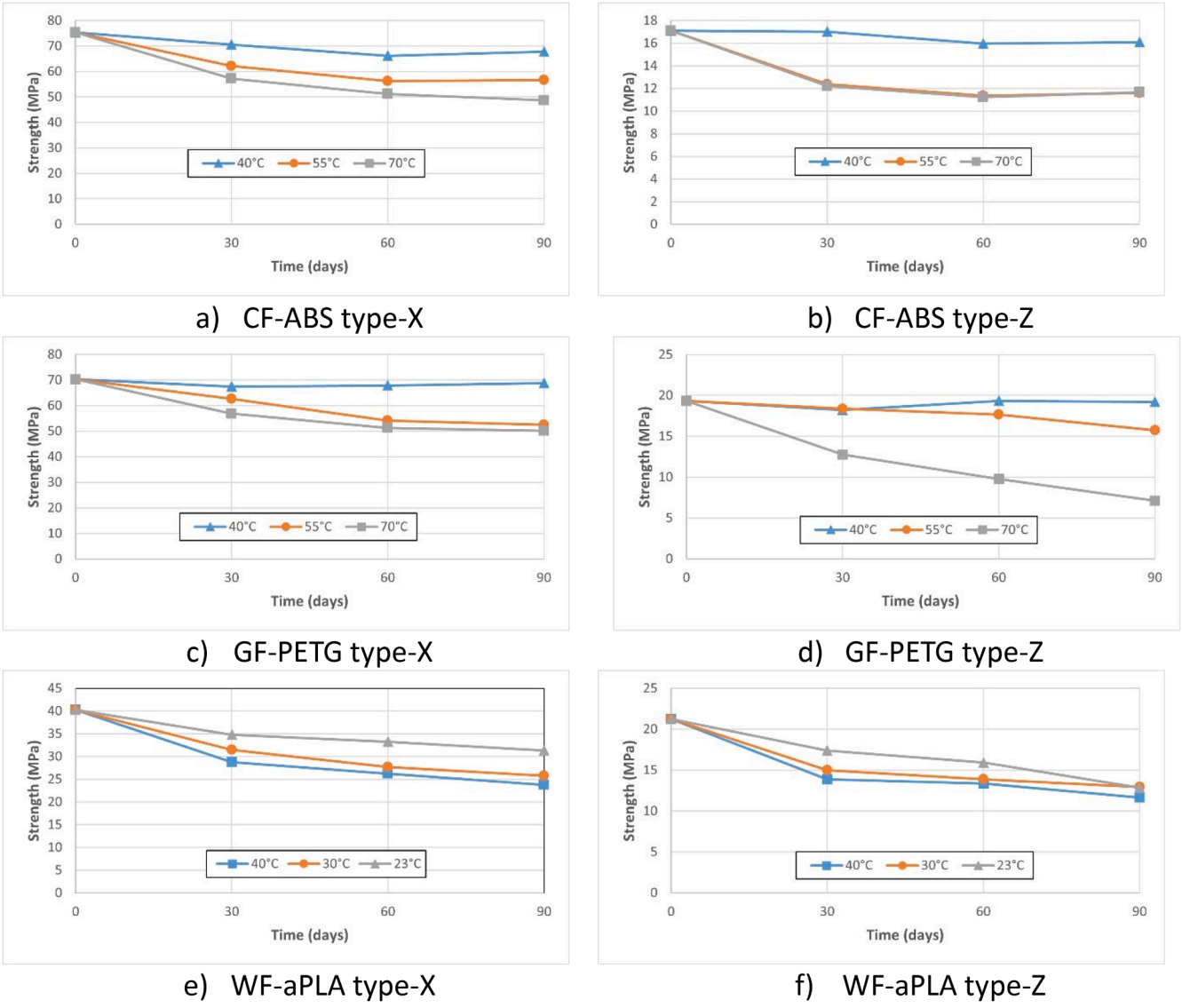

Fig. 4. Strength vs time for polymer composite specimens subjected to accelerated water immersion.

hygrothermal aging in Jute/PLA composites, which could be related to changes in mechanical properties: in stage I, the absorption of water leads to plasticization, resulting in increased ductility while reducing strength and tensile elastic modulus, with no noticeable change in the microstructure, in stage II, cracks form between the fiber and matrix due to differential swelling and interface weakening, significantly harming the mechanical properties and in stage III, matrix hydrolysis induces microcracking, causing a further substantial reduction in ductility. Similar observations were made by Zhao et al. [18], where the fracture mode of another thermoplastic polymer polyethylene terephthalate glycol (PETG) changed from brittle to ductile, indicating absorption of water leading to plasticization.

Fig. 7 presents the rate of degradation as a function of inverse of temperature for the different polymer composite specimens. Stage I shows good correlation between the degradation vs inverse of temperature, supporting the existence of Arrhenius type-relation, suggesting that increasing the temperature increases the rate of polymer composite degradation. However, in stage II, the Arrhenius relationship does not hold true, suggesting that the polymer degradation is more complex and the strength reduction is not only due to increased rate of reaction. Further studies are required to understand the polymer composite degradation and strength reduction at stage II and to model the strength reduction.

The low R^2 value of 0.37 suggests the degradation model does not fit with the Arrhenius equation. This result indicates there was no significant degradation at 40 °C, and therefore, a prediction for CF-ABS type-Z specimens was not applicable.

Fig. 8 shows the predicted and measured mean strength of the polymer composite specimens after water immersion. The predictions are based on the first stage of degradation, i.e., the first 30 days of water immersion.

Based on the prediction plots, the predicted mean strength is comparatively lower than the measured mean strength. The prediction of mean strength using Arrhenius relationship was only possible for a short duration of time.

Discussion on degradation mechanisms

The results of this study indicate that LFAM polymer composites degrade through a combination of chemical and mechanical processes during prolonged water immersion. The extent and rate of these mechanisms depend strongly on the polymer chemistry and the build orientation of the specimens.

Chemical degradation was most evident in the bio-based WF-aPLA, where a 64 % reduction in mean molecular weight and a 69 % increase

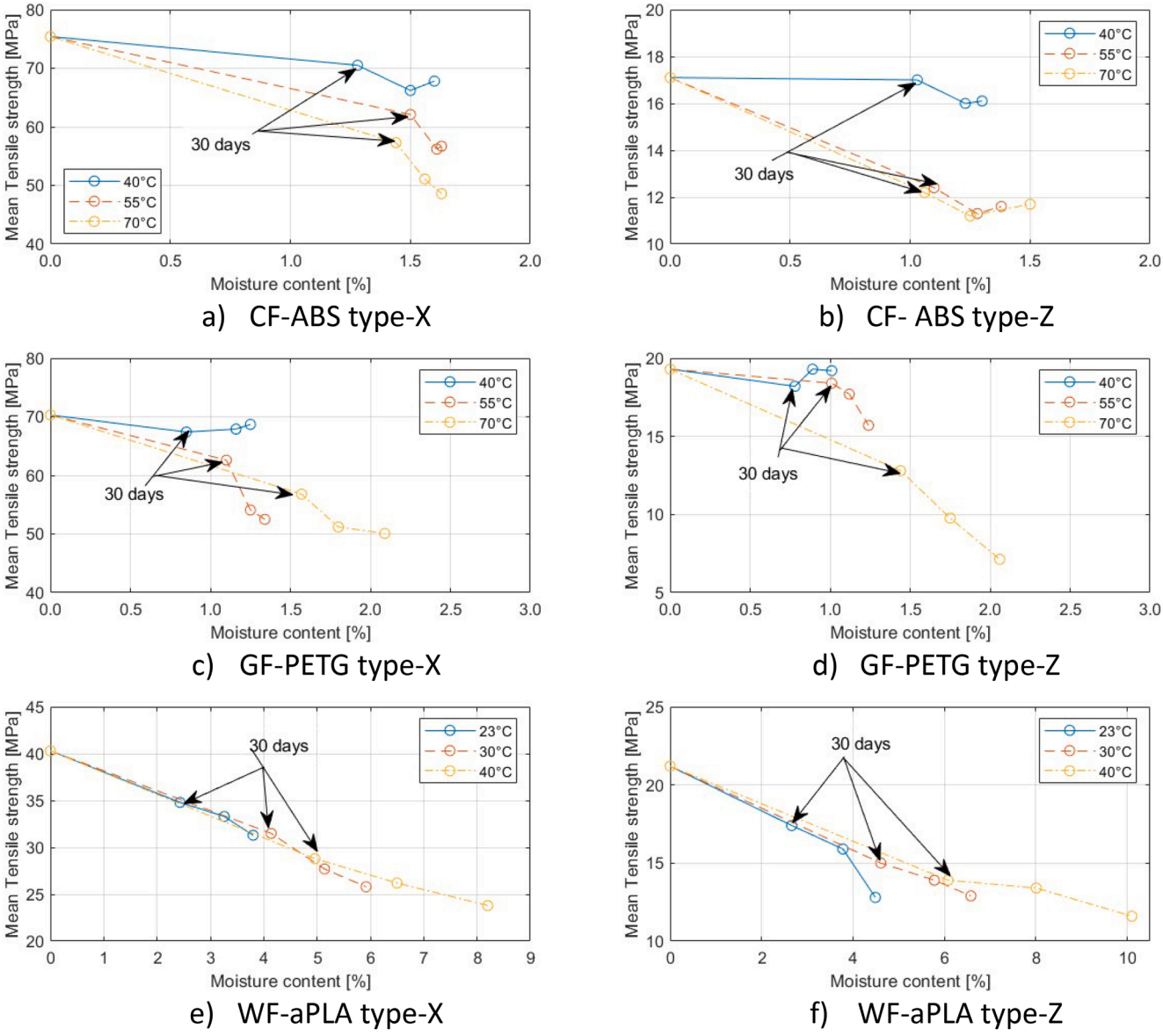

Fig. 5. Strength vs moisture content for polymer composite specimens subjected to accelerated water immersion.

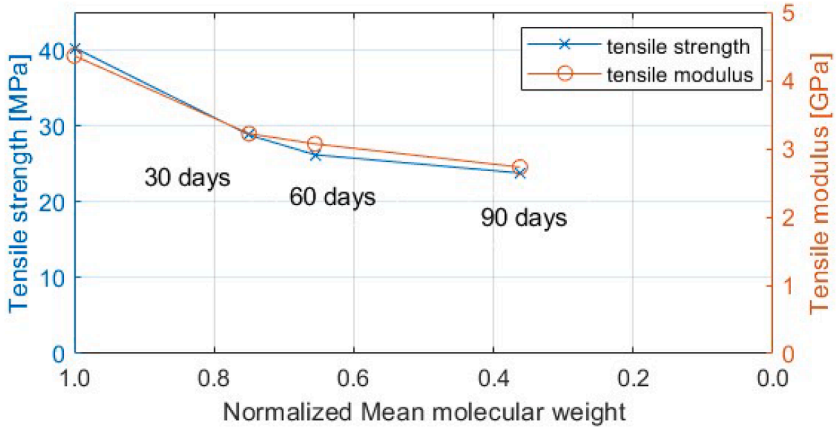

Fig. 6. Mean molecular weight vs tensile strength and modulus for WF-aPLA type-X specimens.

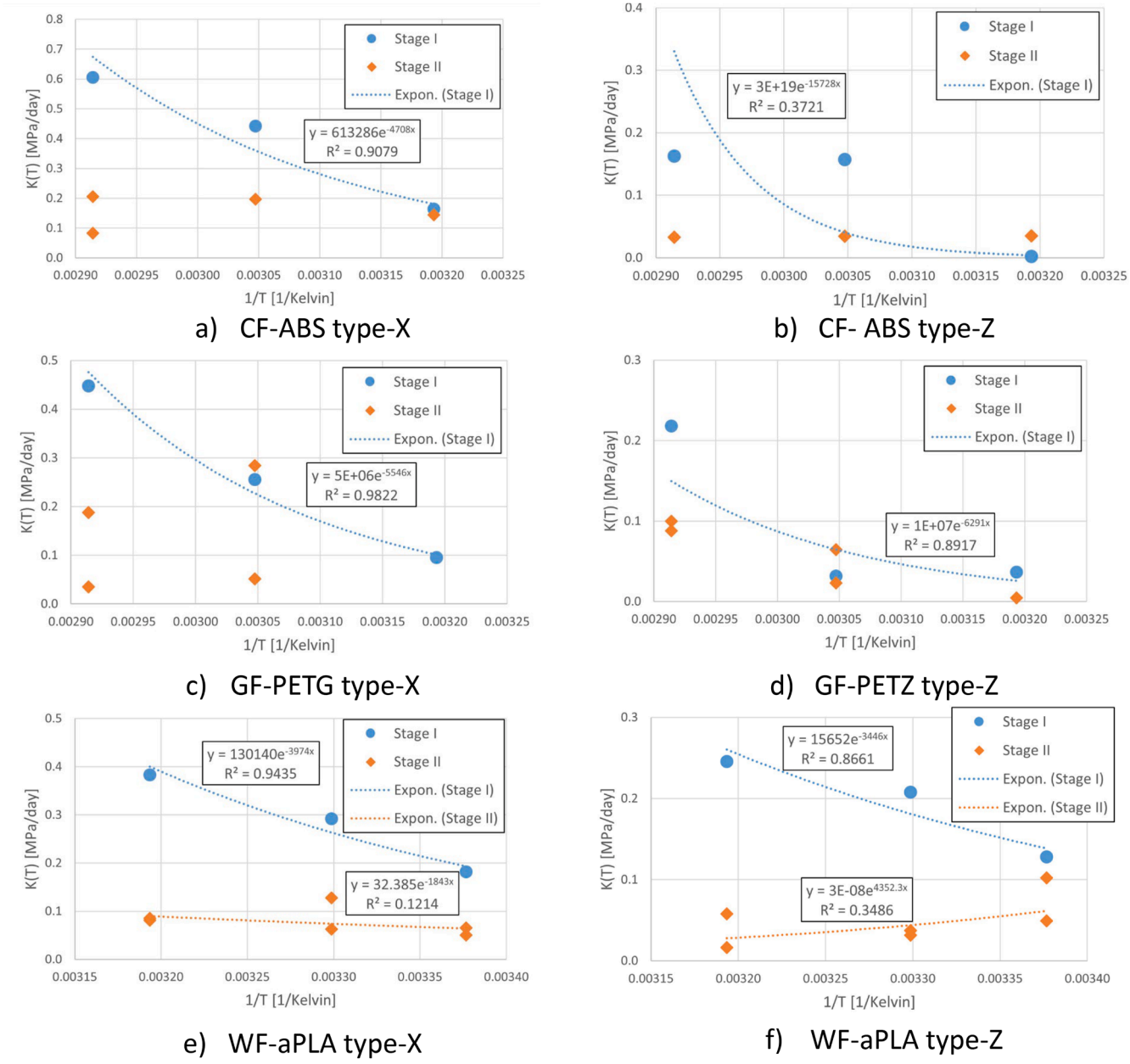

Fig. 7. Rate of degradation vs 1/temperature for polymer composite specimens.

in polydispersity were observed after 90 days of immersion at 40 °C. This indicates significant chain scission and hydrolytic cleavage of the PLA backbone, a degradation pathway well-documented for aliphatic polyesters [45–47]. GF-PETG also exhibited molecular weight reduction (~20 %), consistent with partial hydrolysis of ester linkages, whereas CF-ABS showed relatively minor changes (~4 %), reflecting the greater hydrolytic stability of petroleum-based ABS. The reduction in specific gravity for WF-aPLA further suggests void formation and mass loss associated with polymer degradation, providing additional evidence of chemical weakening of the polymer matrix.

Mechanical degradation manifested as strength and stiffness losses, particularly in Z-direction specimens, where a greater number of interlayer interfaces and voids were present. This anisotropic behavior suggests that moisture ingress accelerates interfacial debonding and void coalescence at LFAM bead boundaries. In WF-aPLA, chemical degradation and void formation compounded the mechanical weakening, resulting in up to 45 % loss in tensile strength and 40 % reduction in tensile modulus. In contrast, CF-ABS and GF-PETG retained much of their stiffness but exhibited progressive strength reduction, likely due to fiber–matrix debonding and interface softening, rather than bulk matrix failure.

The degradation process occurred in two stages. An initial rapid stage was observed within the first 30 days, where water uptake caused plasticization of the polymer matrix, reduction in strength, and weakening of bead interfaces. This stage followed an Arrhenius-type temperature dependence, indicating a reaction-rate controlled process. A secondary slower stage followed, where further reductions in molecular weight, microcrack formation, and progressive fiber–matrix debonding occurred. The slower kinetics and deviation from Arrhenius behavior suggest that multiple degradation mechanisms of hydrolysis, microcracking, and interfacial weakening interact in this stage, making it more complex to predict with conventional models.

Together, these findings show that LFAM composites are susceptible to both chemical hydrolysis of the polymer matrix and mechanical degradation driven by moisture-assisted interfacial failure, with bio-based polymers being especially vulnerable. The distinct two-stage

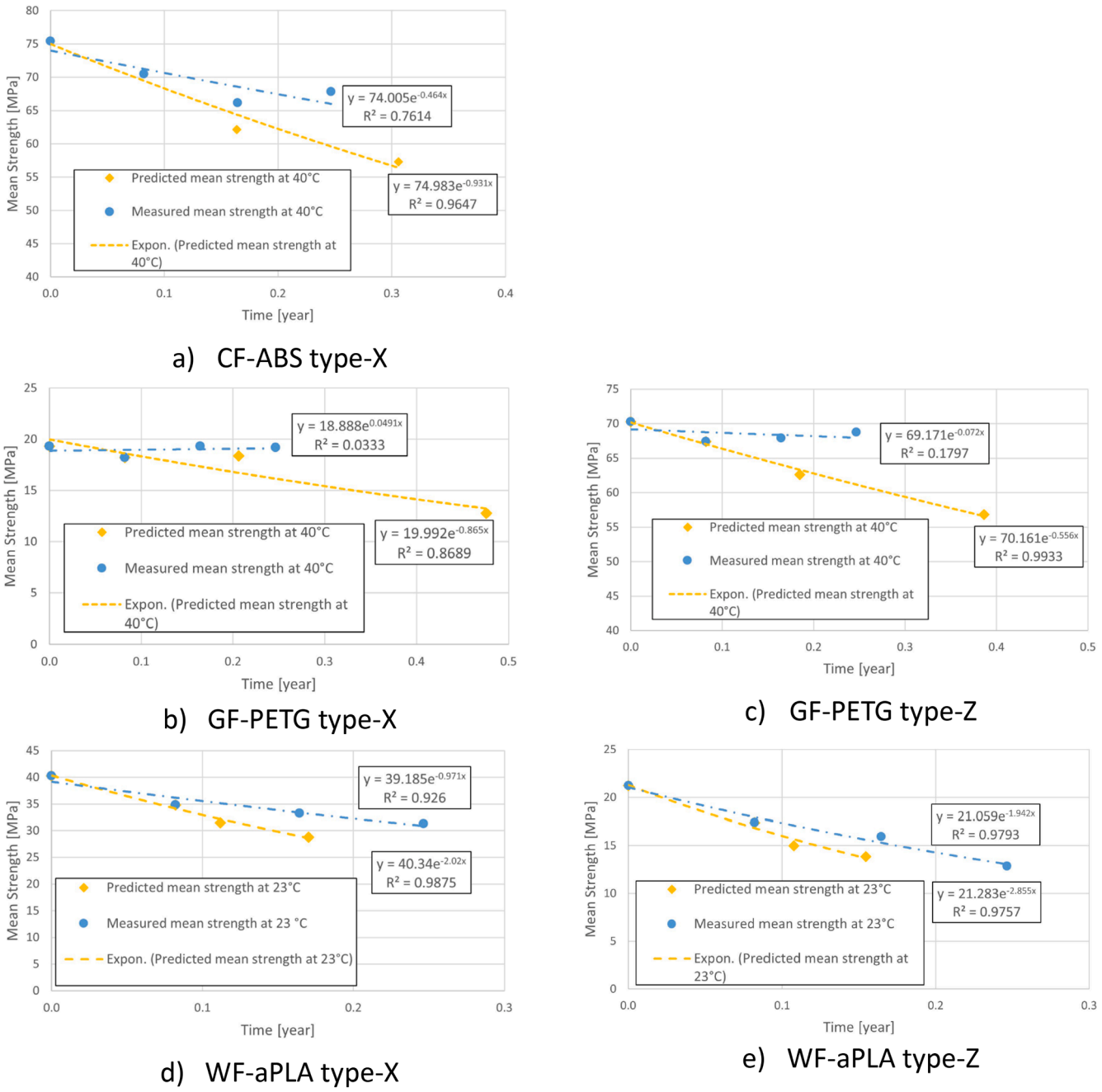

Fig. 8. Predicted and measured mean strength after water immersion for polymer composite specimens.

degradation pattern underscores the need for durability models that account for coupled chemical and mechanical processes rather than relying solely on single-mechanism Arrhenius extrapolations.

Conclusions

The following conclusions were drawn from the study:

1. The durability of LFAM polymer composites exposed to moisture was studied using accelerated water immersion. It was observed that conventional petroleum-based polymer composites are more durable compared to bio-based polymers. The bio-based polymers absorbed moisture and underwent molecular degradation, which resulted in the specimens never reaching the moisture equilibrium. The type-Z specimens, with a greater number of interfaces, were less durable compared to the longitudinal specimens.
2. The loss in mechanical properties of the specimens was characterized. It was observed that the bio-based polymer composites had a significant loss in mechanical properties. The loss in mechanical properties was greater for the type-Z specimens, with a greater number of interfaces.
3. It was observed that the strength reduction occurred in stages. The first stage showed rapid degradation, and the rate of degradation followed the Arrhenius model with respect to the inverse of temperature. The predictions on the strength reductions based on stage I of degradation tend to overpredict the loss of strength. The second stage of degradation was slower and could not be modeled properly using the Arrhenius model, indicating a need for more sophisticated

models that account for degradation mechanisms other than the increased rate of reaction at elevated temperatures.

CRediT authorship contribution statement

Sunil Bhandari: Writing – review & editing, Writing – original draft, Supervision, Methodology, Investigation, Conceptualization. **Prabhat Khanal:** Visualization, Methodology, Investigation, Data curation, Conceptualization. **Roberto A. Lopez-Anido:** Writing – review & editing, Supervision, Methodology, Investigation, Funding acquisition, Conceptualization.

Declaration of competing interest

The authors declare that they have no known competing financial interests or personal relationships that could have appeared to influence the work reported in this paper.

Acknowledgements

The work presented in the paper was done with support from the Transportation Infrastructure Durability Center at the University of Maine under grant 69A3551847101 from the U.S. Department of Transportation's University Transportation Centers Program and the USDOT ARPA-I program, as a part of the X-BRIDGE Program. The authors would like to thank Dr. W. Gramlich and Dr. D. Bones of the Department of Chemistry at the University of Maine for their help with GPC.

Data availability

Data will be made available on request.

References

[1] J. Shah, et al., Large-scale 3D printers for additive manufacturing: design considerations and challenges, Int. J. Adv. Manuf. Technol. 104 (9–12) (2019) 3679–3693.
[2] D. Moreno Nieto, S.I. Molina, Large-format fused deposition additive manufacturing: a review, Rapid Prototyp. J. 26 (5) (2020) 793–799.
[3] C.M.S. Vicente, et al., Large-format additive manufacturing of polymer extrusion-based deposition systems: review and applications, Prog. Addit. Manuf. 8 (6) (2023) 1257–1280.
[4] Najmon, J.C., S. Raeisi, and A. Tovar, *Review of additive manufacturing technologies and applications in the aerospace industry.* 2019: p. 7–31.
[5] P. Chambon, et al., Development of a range-extended electric vehicle powertrain for an integrated energy systems research printed utility vehicle, Appl. Energy 191 (2017) 99–110.
[6] J.M. Jafferson, H. Sharma, Design of 3D printable airless tyres using NTopology, Mater. Today: Proc. 46 (2021) 1147–1160.
[7] M. Ziółkowski, T. Dyl, Possible applications of additive manufacturing technologies in shipbuilding: a review, Machines 8 (4) (2020) 84.
[8] S. Bhandari, et al., Large-scale extrusion-based 3D printing for highway culvert rehabilitation. SPE-ANTEC-2021, Society of Plastics Engineers: Virtual, 2021.
[9] Bhandari, S., et al., *Design and manufacture of precast concrete formworks using polymer extrusion-based large-scale additive manufacturing and postprocessing.* 2022: p. 1–13.
[10] Love, L.J., *Utility of big area additive manufacturing (BAAM) for the rapid manufacture of customized electric vehicles.* 2015(1209199).
[11] C.E. Duty, et al., Structure and mechanical behavior of Big Area Additive Manufacturing (BAAM) materials, Rapid Prototyp. J. 23 (1) (2017) 181–189.
[12] C. Ajinjeru, et al., Rheological survey of carbon fiber-reinforced high-temperature thermoplastics for big area additive manufacturing tooling applications, J. Thermoplast. Compos. Mater. 34 (11) (2019) 1443–1461.
[13] Post, B., et al., *The economics of big area additive manufacturing.* 2016.
[14] R. Lopez-Anido, et al., Overview of thermoplastic composites in bridge applications, in: European Bridge Conference-2022, Edinburgh, UK, 2022.
[15] N.M. Stark, D.J. Gardner, Outdoor Durab. Wood–Polym. Compos. (2008) 142–165.
[16] F. Pomies, L.A. Carlsson, Analysis of modulus and strength of dry and wet thermoset and thermoplastic composites loaded in transverse tension, J. Compos. Mater. 28 (1) (1994) 22–35.
[17] P. Zhou, et al., Comparative study of durability behaviors of thermoplastic polypropylene and thermosetting epoxy exposed to elevated temperature, water immersion and sustained bending loading, Polymers (Basel) (14) (2022) 14.
[18] X. Zhao, et al., Hygrothermal aging behavior and mechanical degradation of ramie/carbon fiber reinforced thermoplastic polymer hybrid composites, Ind. Crops Prod. 193 (2023) 116212.
[19] P. Ghabezi, et al., Degradation characteristics of 3D printed continuous fibre-reinforced PA6/chopped fibre composites in simulated saltwater, Prog. Addit. Manuf. 10 (1) (2025) 725–738.
[20] A.D. Banjo, et al., Moisture-induced changes in the mechanical behavior of 3D printed polymers, Compos. C: Open Access 7 (2022) 100243.
[21] A. Elmushyakhi, Freeze-thaw stabilization of fused deposition modeling 3D-printed SABIC structures, J. King Saud Univ. - Eng. Sci. 34 (2) (2022) 116–125.
[22] M. Pizzorni, M. Prato, Effects of hygrothermal aging on the tensile and bonding performance of consolidated 3D printed polyamide-6 composites reinforced with short and multidirectional continuous carbon fibers, Compos. A: Appl. Sci. Manuf. 165 (2023) 107334.
[23] F.A. Saavedra-Rojas, S. Bhandari, R.A. Lopez-Anido, Environmental durability of bio-based and synthetic thermoplastic composites in large-format additive manufacturing, Polymers (Basel) (6) (2024) 16.
[24] D3039 Standard Test Method for Tensile Properties of Polymer Matrix Composite Materials, ASTM International, West Conshohocken, PA, USA, 2017, 100 Barr Harbor Drive, PO Box C700.
[25] B. Khoda, et al., Effect of molecular weight on polymer solution facilitated transfer of non-Brownian particles, Prog. Org. Coat. 176 (2023) 107394.
[26] K. Schweizer, et al., Recycling large-format 3D printed polymer composite formworks used for casting precast concrete – technical feasibility and challenges, J. Compos. Constr. (6) (2024) 28.
[27] N. Jiang, et al., Hygrothermal aging and structural damage of a jute/poly (lactic acid) (PLA) composite observed by X-ray tomography, Compos. Sci. Technol. 173 (2019) 15–23.
[28] A. Patti, et al., Aging Effects On the Viscoelastic Behaviour of Products By Fused Deposition Modelling (FDM) Made from Recycled and Wood-Filled Polymer Resins, 82, European Journal of Wood and Wood Products, 2023, pp. 69–79.
[29] A. Regazzi, et al., Reversible and irreversible changes in physical and mechanical properties of biocomposites during hydrothermal aging, Ind. Crops Prod. 84 (2016) 358–365.
[30] J.L. Colon Quintana, et al., Effects of Fiber Orientation on the Coefficient of Thermal Expansion of Fiber-Filled Polymer Systems in Large Format Polymer Extrusion-Based Additive Manufacturing, Materials (Basel) (8) (2022) 15.
[31] D5229 Standard Test Method for Moisture Absorption Properties and Equilibrium Conditioning of Polymer Matrix Composite Materials, A. International, West Conshohocken, PA, USA, 2020. Editor.100 Barr Harbor Drive, PO Box C700.
[32] Wolf, A.T., *Effects of water immersion on building and civil engineering joints and the use of the arrhenius method in predicting adhesion lifetime of water-immersed joints.* 2010: p. 111–111-24.
[33] K.J. Hemmerich, General aging theory and simplified protocol for accelerated aging of medical devices, Med. Plast. Biomater. 5 (1998) 16–23.
[34] D.H. Collins, et al., Accelerated test methods for reliability prediction, J. Qual. Technol. 45 (3) (2017) 244–259.
[35] O. Starkova, et al., Modelling of environmental ageing of polymers and polymer composites-durability prediction methods, Polymers (Basel) 14 (5) (2022).
[36] J. Wang, et al., Durability and prediction models of fiber-reinforced polymer composites under various environmental conditions: a critical review, J. Reinf. Plast. Compos. 35 (3) (2015) 179–211.
[37] A. Plota, A. Masek, Lifetime prediction methods for degradable polymeric materials-a short review, Materials (Basel) (20) (2020) 13.
[38] J.F. Davalos, Y. Chen, I. Ray, Long-term durability prediction models for GFRP bars in concrete environment, J. Compos. Mater. 46 (16) (2011) 1899–1914.
[39] L.C. Bank, et al., A model specification for FRP composites for civil engineering structures, Constr. Build. Mater. 17 (6–7) (2003) 405–437.
[40] M.A.G. Silva, B.S. da Fonseca, H. Biscaia, On estimates of durability of FRP based on accelerated tests, Compos. Struct. 116 (2014) 377–387.
[41] G. Wu, et al., Prediction of long-term performance and durability of BFRP bars under the combined effect of sustained load and corrosive solutions, J. Compos. Constr. 19 (3) (2015).
[42] V. Dejke, Durability of FRP Reinforcement in Concrete, Chalmers University of Technology: Göteborg, Sweden, 2001.
[43] W.B. Nelson, Accelerated Testing: Statistical Models, Test Plans, and Data Analysis, John Wiley & Sons, 2009.
[44] B. Yu, et al., Interfacial and glass transition properties of surface-treated carbon fiber reinforced polymer composites under hygrothermal conditions, Eng. Sci. (2018).
[45] Teixeira, S., et al., *Towards controlled degradation of poly(lactic) acid in technical applications.* C, 2021. 7(2): p. 42.
[46] C. Valverde, et al., Hydrolytic and enzymatic degradation studies of aliphatic 10-undecenoic acid-based polyesters, Polym. Degrad. Stab 155 (2018) 84–94.
[47] R. Vaid, et al., Hydrolytic degradation of polylactic acid fibers as a function of pH and exposure time, Molecules (24) (2021) 26.

polymers

MDPI

Article

Environmental Durability of Bio-Based and Synthetic Thermoplastic Composites in Large-Format Additive Manufacturing

Felipe A. Saavedra-Rojas [1,2], Sunil Bhandari [1,2,*] and Roberto A. Lopez-Anido [1,2]

[1] Advanced Structures and Composite Center, University of Maine, Orono, ME 04469, USA; felipe.saavedra@maine.edu (F.A.S.-R.); rla@maine.edu (R.A.L.-A.)
[2] Department of Civil and Environmental Engineering, University of Maine, Orono, ME 04469, USA
* Correspondence: sunil.bhandari@maine.edu

Abstract: This research investigates the durability of large-format 3D-printed thermoplastic composite material systems under environmental exposure conditions of moisture and freeze–thaw. Durability was evaluated for two bio-based composite material systems, namely wood-fiber-reinforced semi-crystalline polylactic acid (WF/PLA) and wood-fiber-reinforced amorphous polylactic acid (WF/aPLA), and one conventionally used synthetic material system, namely short-carbon-fiber-reinforced acrylonitrile butadiene styrene (CF/ABS). The moisture absorption, coefficient of moisture expansion, and reduction of relevant mechanical properties—flexural strength and flexural modulus—after accelerated exposure were experimentally characterized. The results showed that the large-format 3D-printed parts made from bio-based thermoplastic polymer composites, compared to conventional polymer composites, were more susceptible to moisture and freeze–thaw exposure, with higher moisture absorption and greater reductions in mechanical properties.

Keywords: large-format additive manufacturing; 3D printing; durability; accelerated testing; moisture; freeze–thaw; composite; bio-based; carbon fiber

Citation: Saavedra-Rojas, F.A.; Bhandari, S.; Lopez-Anido, R.A. Environmental Durability of Bio-Based and Synthetic Thermoplastic Composites in Large-Format Additive Manufacturing. *Polymers* **2024**, *16*, 787. https://doi.org/10.3390/polym16060787

Academic Editor: Qinghua Wei

Received: 20 January 2024
Revised: 27 February 2024
Accepted: 4 March 2024
Published: 12 March 2024

1. Introduction

In recent years, the use of additive manufacturing (AM) to make functional products has increased significantly. The expansion of 3D printing technology to include larger-scale capabilities has the potential to revolutionize various industries by offering more efficient, cost-effective, and flexible manufacturing solutions [1]. Bishop et al. [2] highlighted the usage of large-format additive manufacturing for rapid manufacturing processes in response to emergency shortages. Roschli et al. [3] demonstrated the use of precast concrete molds fabricated for casting architectural building components using additive manufacturing. Bhandari et al. presented the use of 3D-printed formworks for a precast concrete pier cap of a highway bridge [4], formworks for window openings for a precast concrete parking garage wall system [5], and formworks for casting precast concrete ballast retainers for railroad bridges [6]. Peters [7] studied the potential and advantages of flexible formwork for precast concrete architectural applications, showing that it can be implemented immediately in the construction industry since it improves an already known technique and material.

Large-format AM has also been used to manufacture polymer composite structures that are expected to last for long timespans. Bhandari et al. [8] demonstrated the use of 3D-printed diffusers for the rehabilitation of highway culverts. The University of Maine and Oak Ridge National Laboratory collaborated to design and manufacture a bio-based additively manufactured house prototype known as BioHome3D [9]. Liedtka [10] evaluated the life cycle, embodied energy, and sustainability potential for large-format additive manufacturing of 3D-printed modular houses. Conventional polymer composite systems

derived from petroleum products as well as novel bio-based polymer composite systems are being used as feedstock material in large-format additive manufacturing. Van de Werken et al. [11] reviewed the use and effectiveness of short carbon fiber reinforcement in different polymer composite systems, used as a feedstock material in large-format additive manufacturing. Zhao et al. [12] used poplar-biofiber-reinforced polylactic acid (PLA) to manufacture podium supports and found that the porous and hollow microstructures in poplar fibers enabled better interfacial bonding with the PLA polymer. Lamm et al. [13] reviewed the use of natural fillers in the polymer composite systems used in large-format additive manufacturing.

The increasing adoption of large-format AM for the manufacturing of long-standing structures with outdoor exposure has necessitated the development of a better understanding of the mechanical durability of large-format extrusion-based AM-produced polymer composite parts [14]. Specifically, the durability of a material or structure is summarized as "its ability to resist cracking, oxidation, chemical degradation, delamination, wear, and/or the effects of foreign object damage for a specified period, under the appropriate load conditions, under specified environmental conditions" [15]. The durability of various conventionally manufactured synthetic as well as bio-based polymer composites has been well studied. The durability of polymer composites is divided into two broad categories: structural durability and aesthetic durability [16]. Both categories are important since, from the structural durability point of view, polymer composites need to withstand service loads while, at the same time, maintaining the required aesthetics during their service life. From the structural point of view, durability can be defined as the ability of a building structure to remain fit for the design purpose during its service life [17]. Accelerated testing uses several test techniques to cut the lifespan of products or speed up the performance degradation of such products [18]. Stamboulis et al. [19] studied the durability of compression-molded flax-fiber-reinforced polypropylene composites. Stark et al. [20] studied the outdoor durability of wood polymer composites (WPC) made of high-density polyethylene (HDPE) with 50% wood flour, comparing extruded, compression-molded, and injection-molded WPC. For moisture, the hydroxyl groups on wood or other lignocellulosic materials are primarily responsible for water absorption. As the wood particle absorbs moisture, it swells, producing stresses in the WPC matrix and creating microcracks. Swelling also creates stress in the wood particles. Once the material is dried, there is no adhesion at the matrix and wood particle interface, creating voids that water will penetrate during later exposure, affecting its durability. In a ten-year field study, Gardner et al. [21] inserted stakes made of polypropylene (PP) with 49–52% wood flour in the ground to evaluate decay, termite ratings, surface weathering, biological colonization, and dimensional changes. In addition, flexural tests were conducted to evaluate the flexural properties after ten years, showing a decrease or no change depending on the composite formulation. Malpot et al. [22] investigated the effect of moisture ingress on the fatigue behavior of glass-fiber-reinforced polyamide manufactured using resin transfer molding. The study found that moisture ingress significantly increased the fiber fracture for fatigue loadings with medium to high stress ratios. Pomies and Carlsson [23] studied the effect of moisture on injection-molded glass-fiber-reinforced polyphenylene sulfide and found degradation in the fiber–matrix interface due to moisture ingress.

Researchers have studied the environmental durability of desktop-scale 3D-printed thermoplastic composites. Celestine et al. [24] studied the mechanical moisture-ingress-induced degradation of 3D-printed and injection-molded nylon polymer parts. The study found that the rate of absorption for the 3D-printed specimens was higher than that of the injection-molded specimens. Cormier and Poddar [25] highlighted that printing voids, the interlayer bond strength, and the fiber strength affect the durability of parts fabricated via additive manufacturing. These properties are influenced by the processing settings and material selection. The material structure in large-format polymer-extrusion-based 3D parts makes the material more susceptible to moisture absorption and water ingress, which affects the durability. Banjo et al. [26] reported a high water absorption rate for

desktop-scale 3D-printed nylon and PLA and corresponding physical and mechanical property degradation, when immersed in water at high temperatures of 70 °C. However, the loss in mechanical properties was negligible when the immersion was at a temperature of 20 °C. Kaknuru and Pochiraju [27] studied the uptake of moisture in desktop-scale 3D-printed ABS and PLA polymers and highlighted the effects of moisture penetration on the mechanical properties of the 3D-printed parts. Xiao et al. [28] studied the degradation in the mechanical properties of 3D-printed polyethylene due to exposure to ultraviolet radiation and found that such exposure caused a reduction in tensile strength, modulus, ductility, and toughness. Dizon et al. [29] studied the effect of post-processing on 3D-printed polymer composite parts and found that post-processing could be used to improve the durability of such parts. Afshar and Mihut [30] found that the durability of 3D-printed polymer composite parts could be improved by depositing a thin metallic copper film on the surface of the 3D-printed parts. Glowacki et al. [31] studied the effect of freeze–thaw cycling on the durability of 3D-printed acrylonitrile butadiene styrene and polylactic acid and found that one cycle lasting seven days was enough to alter the mechanical properties of the materials.

Although studies have been carried out to investigate the durability of thermoplastic polymer composites manufactured using desktop-scale 3D printing, the durability of thermoplastic composite materials manufactured with large-format 3D printing needs further investigation. Grassi et al. [32] studied the durability of wood-fiber-reinforced polylactic acid and polypropylene for desert climates. The study focused on the durability of large-format 3D-printed structures against thermal and ultraviolet exposure. Large-scale 3D-printed parts for exterior use are exposed to freeze–thaw cycles and moisture. This exposure affects the durability of the part in service. The voids and imperfect fusion between layers and the micro-porosity within the beads are more pronounced in parts manufactured with large-format additive manufacturing [33]. Such a material structure in large-format polymer-extrusion-based 3D parts makes the material more susceptible to moisture absorption and water ingress, which affects the durability. Hence, a durability study of large-format 3D-printed polymer composite materials is necessary to evaluate their use and guide the design of long-standing structures.

The objectives of this study are to

1. Investigate the moisture absorption behavior of bio-based and synthetic polymer composites manufactured using large-format additive manufacturing;
2. Evaluate the dimensional changes of bio-based 3D-printed polymer composites caused by moisture ingress;
3. Characterize the mechanical property degradation of large-format 3D-printed bio-based and synthetic polymer composites due to moisture ingress; and
4. Characterize the mechanical property degradation of large-format 3D-printed bio-based and synthetic polymer composites due to freeze–thaw cycling.

2. Materials and Methods

2.1. Materials and Sample Preparation

2.1.1. Materials

This study used two bio-based polymer composites and a synthetic polymer composite.

- WF/PLA, or wood fiber (WF)-reinforced polylactic acid (PLA), is a bio-based polymer composite with a conventional semi-crystalline PLA polymer. HiFill PLA 1816 3DP with 20% fiber reinforcement by weight, supplied by Techmer PM, Clinton, TN, USA, was used as the feedstock material for large-format 3D printing.
- WF/aPLA, or WF-reinforced amorphous PLA, is a bio-based polymer composite with a novel amorphous PLA polymer. PLA 3120 WF PEL with 20% fiber reinforcement by weight, supplied by Jabil, Chaska, MN, USA, was used as the feedstock material for large-format 3D printing.
- CF/ABS, or short-carbon-fiber-reinforced acrylonitrile butadiene styrene (ABS), is a synthetic material system with a petroleum-derived ABS polymer. Electrafil ABS 1501

3DP with 20% fiber reinforcement by weight, supplied by Techmer PM, Clinton, TN, USA, was used as the feedstock material for large-format 3D printing.

The 3D-printed parts exhibited orthotropic mechanical behavior [34,35]. Figure 1 shows the principal material direction convention adopted for the large-format 3D-printed specimens. Direction 1 is along the bead, direction 2 is perpendicular to the bead in the same plane of deposition, and direction 3 is normal to the plane of deposition.

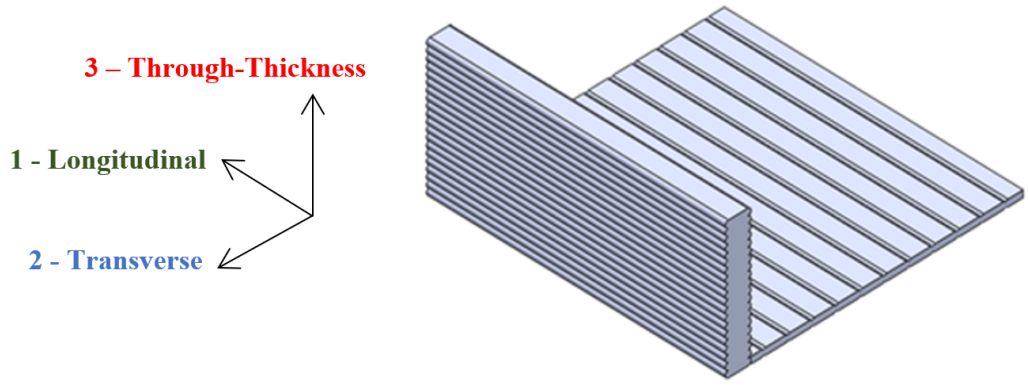

Figure 1. Material direction convention adopted for large-format 3D-printed specimens.

2.1.2. Specimen Preparation

The 3D-printed panels were manufactured using large-format 3D printing using the Ingersoll Masterprint 3D printing equipment. A bead width of 19.1 mm (0.75 inches) and a bead height of 5.08 mm (0.20 inch) were used for the manufacturing of the specimens. The extrusion temperature at the nozzle for CF/ABS, WF/PLA, and WF/aPLA was 240 °C, 207 °C, and 210 °C, respectively. Figure 2 shows the principal material directions in the specimen. The specimens were 196 mm long, 38.2 mm wide, and 10.2 mm thick. The specimens were two beads thick and two beads wide. The specimens consisted of at least one interlayer interface and one intralayer interface, so that the effect of the interface on water ingress, hygroscopic expansion, and mechanical properties was taken into account.

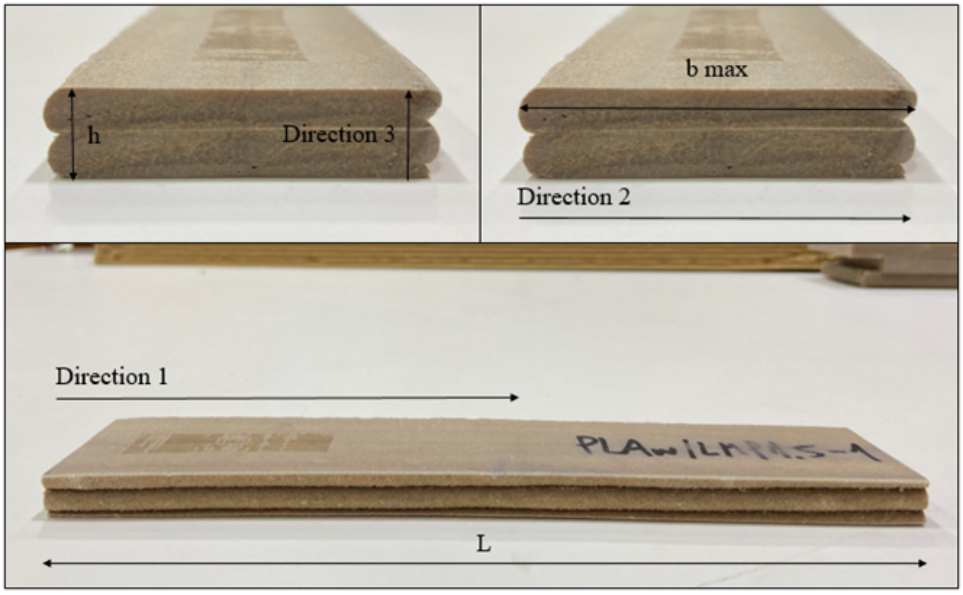

Figure 2. The 3D-printed specimens with dimensions and material direction.

2.2. Experimental Methods

Three sets of 3D-printed specimens were prepared. Each set consisted of three different materials. The first set of 3D-printed specimens served as the baseline specimens. These baseline specimens were used to characterize the as-printed mechanical properties. The second set of 3D-printed specimens was subjected to accelerated water immersion. The third set of specimens was subjected to freeze–thaw cycling.

2.2.1. Accelerated Water Immersion

The ASTM D5229 [36] test standard was adopted to evaluate the moisture absorption and equilibrium conditioning of the 3D-printed polymer composite specimens. The selected temperature for oven drying and water absorption was 40 °C (below the glass transition temperature (T_g) of WF/PLA 60 °C, being the lowest T_g of the three materials). Specimens were oven-dried at 40 °C for 24 h. Specimens were immersed in distilled water at 40 °C after oven drying, and the conditioning time was 81 days. Moisture content was calculated according to the ASTM D5229 standard. Sorption curves were generated according to the ASTM D5229 standard. The length was measured using a calibrated steel ruler and the width and height were measured using calibrated vernier calipers. The coefficient of moisture expansion (CME) β for the specimens was calculated using Equations (1) and (2) [37,38].

$$\beta = \frac{\varepsilon_H}{M(\%)} \tag{1}$$

$$\varepsilon = \frac{\Delta l}{l_0} \tag{2}$$

where
ε_H = moisture strain;
Δl = change in dimensions of the specimen;
l_0 = initial dimensions;
β = coefficient of moisture expansion for the composite material;
$M(\%)$ = specimen moisture content as a percentage.

2.2.2. Freeze–Thaw Cycling

Freeze–thaw cycling was conducted according to ASTM D7992 [39]. A minimum of three specimens were subjected to the freeze–thaw cycles below to determine the effect of freeze–thaw exposure. Test specimens were submerged underwater for 24 h. The specimens were then placed in a freezer at −29 °C (−20 °F) for 24 h. After being frozen, the specimens were returned to room temperature for 24 h. This process comprised one hygrothermal cycle. The procedure was repeated two more times for a total of three cycles of water submersion, freezing, and thawing. After three freeze–thaw cycles, the specimens were allowed to return to room temperature, followed by flexure testing.

2.3. Evaluation of Mechanical Properties Using Flexure Tests

Procedure B of the ASTM D7264 standard test method [40] was adopted to evaluate the flexural modulus and flexural strength of the specimens. A beam specimen with a rectangular cross-section was simply supported and loaded in four-point bending. A constant displacement rate of 4.34 mm/min was adopted. Figure 3 illustrates the loading configuration and the principal material axes of the beam specimen. The specimen was loaded in flexure along the direction of the deposited beads (direction—1). The length of the specimen was 196 mm, the width was 38.2 mm, and the height was 10.2 mm. The specimen dimensions were selected based on the bead geometry of the 3D-printed parts, with the width of the flexure test specimen equal to the width of two extruded beads and the specimen height equal to the thickness of two extruded beads. The loaded span was 180 mm with an 8 mm overhang on both sides. The loads were applied at a distance of 90 mm from the supports.

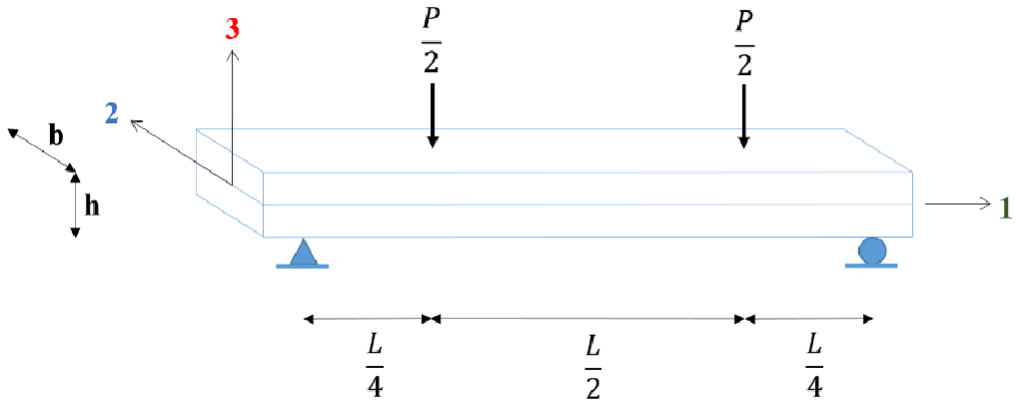

Figure 3. Beam specimen loading configuration and material directions.

An ARAMIS (v 6.3) 3D-Digital Image Correlation (DIC) system from GOM GmbH, Braunschweig, Germany was used to record the strains on the test specimens' surfaces during testing. The specimens were prepared for the DIC measurement system by placing uncoded white single-point markers of 0.8 mm diameter. Figure 4 shows the single-point markers used for DIC to evaluate the displacements at different locations in the specimens during testing. The displacements were used by the DIC software to calculate the axial strains in the 3D-printed specimens. The flexure tests were performed on a 100 kN servo-hydraulic load frame from Instron, Norwood, MA, equipped with side-loading hydraulic grips, at a temperature of 23 ± 2 °C and 50 ± 5% relative humidity in an environmentally controlled test lab at the Advanced Structures and Composites Center at the University of Maine in Orono, Maine.

Flexural strength was calculated using Equation (3).

$$\sigma_b = \frac{3PL}{4bh^2} \tag{3}$$

where
σ_b = flexural strength;
P = total applied load;
L = beam span;
b = beam width;
h = beam height.

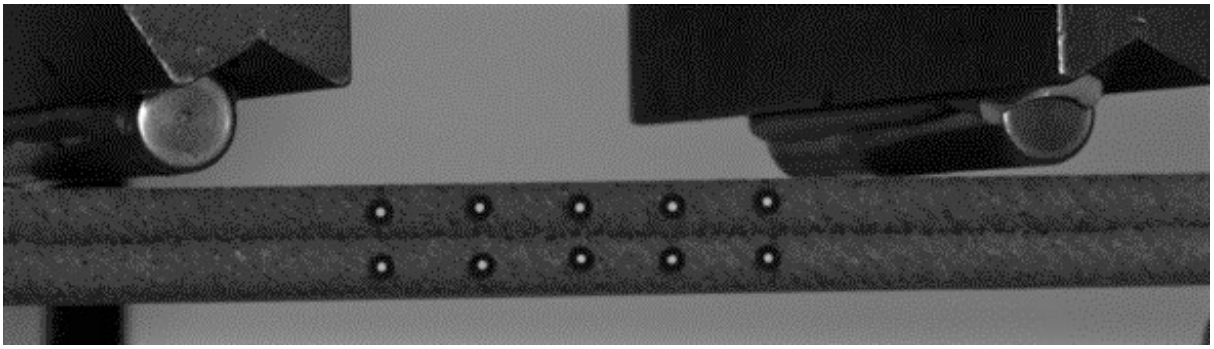

Figure 4. Central span of specimen loaded in four-point bending with single-point markers.

3. Results and Discussion

3.1. Water Immersion Test Results

Moisture diffusion occurred primarily through the surfaces normal to directions 2 and 3 in the specimen. Directions 2 and 3 in relation to the 3D-printed specimens are shown in

Figure 2. The average moisture content measured for WF/PLA, WF/aPLA, and CF/ABS specimens at the end of accelerated moisture exposure are shown in Table 1.

Table 1. Moisture content at the end of accelerated moisture exposure.

Set	Number of Specimens	Average Moisture Content (%)	Coefficient of Variation (%)
WF/PLA	10	7.74	4.08
WF/aPLA	6	9.23	0.72
CF/ABS	6	1.35	7.63

After water immersion for 81 days, WF/aPLA was the material with the highest moisture content of 9.23%, followed by WF/PLA with moisture content of 7.74%, and finally CF/ABS with moisture content of 1.35%. Similar results were observed for WPC- and CF-reinforced polymer composites by other researchers. Wang et al. [41] reported moisture of 10 % to 16 % in different wood plastic composites after water immersion for 200 days. Kim et al. [42] observed moisture absorption of 12% to 16% for different wood polymer composites manufactured using polypropylene and different wood species after water immersion for 100 days. Huang et al. [43] observed moisture absorption of 5% to 6% for different wood polymer composites subjected to water immersion for 40 days.

Sorption curves were generated to visualize the variation in moisture over time. Figure 5 illustrates the sorption curves for WF/PLA, WF/aPLA, and CF/ABS specimens. The bio-based composites gained moisture more rapidly compared to the synthetic polymer composite. WF/aPLA showed the highest rate of increase in moisture with time, followed by WF/PLA. CF/ABS had the lowest rate of water uptake with time. The moisture content of the bio-based polymer composite specimens increased with time and did not reach equilibrium at the end of the testing period. For bio-based polymer composites, the rate of water absorption did not decrease with time. This suggests that mechanisms other than the simple sorption of water by the polymer and reinforcing fiber might have been in action. Jiang et al. [44] reported similar water uptake behavior in conventionally manufactured Jute/PLA composites, where the water uptake of such composites did not reach saturation levels. The research work showed that the water absorption proceeded in three different stages: water absorption by the polymer matrix and wood fiber, crack formation at the matrix–fiber interface, and further microcracking due to the hydrolysis of the matrix. Further study is necessary to identify the cause of this behavior observed in bio-based large-format 3D-printed polymers. The rate of water uptake with time decreased for CF/ABS polymers. The moisture content of CF/ABS specimens increased and approached saturation levels at the end of the testing period. Aniskevich et al. [45] reported similar moisture uptake behavior in 3D-printed ABS polymers.

The coefficients of moisture expansion of the specimens subjected to the accelerated water immersion tests were evaluated. The CF-ABS specimens did not exhibit any change in dimensions when the length was measured with a calibrated ruler and the width and height were measured with vernier calipers. Table 2 shows the coefficient of moisture expansion for WF/aPLA and WF/PLA specimens.

Table 2. Coefficient of moisture expansion for WF/PLA and WF/aPLA specimens.

Material	β_1 (cv)	β_2 (cv)	β_3 (cv)
WF/PLA	2.13×10^{-3} (31%)	2.08×10^{-3} (27%)	5.57×10^{-3} (7.6%)
WF/aPLA	1.83×10^{-3} (10%)	3.26×10^{-3} (3.6%)	5.58×10^{-3} (6.2%)

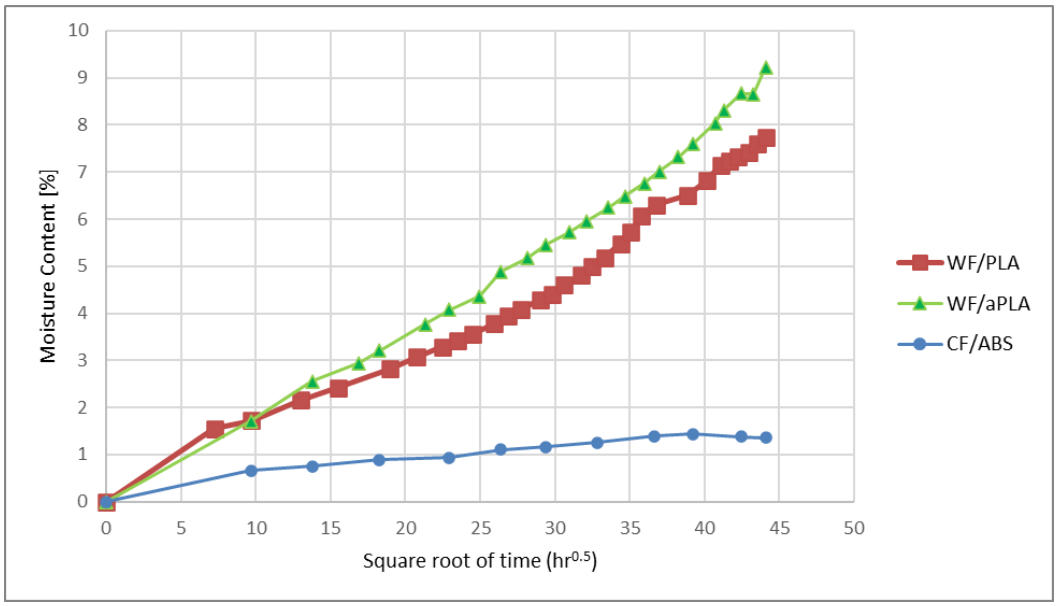

Figure 5. Sorption curves for WF/PLA, WF/aPLA, and CF/ABS.

β_1, β_2, and β_3 are the coefficients of moisture expansion in directions 1, 2, and 3, respectively. The coefficients of moisture expansion showed high values of variation, especially for WF/PLA specimens. In order to compare the CMEs of the materials in different directions and check whether the specimens exhibited orthotropic moisture expansion behavior, an ANOVA test was performed. A p-value of less than 0.05 was considered statistically significant. The results of the ANOVA test are presented in Table 3.

Table 3. Comparison of coefficients of moisture expansion in principal material directions.

Material Directions Compared	p-Value (WF/PLA)	p-Value (WF/aPLA)
β_1, β_2, and β_3	1.87×10^{-14}	9.95×10^{-11}
β_1 and β_2	0.896	3.25×10^{-7}
β_1 and β_3	3.80×10^{-10}	1.51×10^{-8}
β_2 and β_3	3.36×10^{-11}	3.88×10^{-6}

The results from the ANOVA test showed that

- The large-format 3D-printed WF/aPLA exhibited orthotropic moisture expansion behavior, i.e., the CME in each of the three principal material directions was unique;
- The difference between β_1 and β_2 was not statistically significant; the large-format 3D-printed WF/PLA presented in-plane isotropy, with planes 1–2 as the planes of isotropy.

3.2. Flexure Test Results

Baseline Results

Table 4 presents the average flexural strength and flexural modulus of the baseline sets. The number of specimens and the coefficient of variation for strength and moduli calculation are listed in parentheses.

Table 4. Baseline flexural properties of WF/PLA, WF/aPLA, and CF/ABS.

Set	Strength (MPa) (Qty/cv)	Modulus (GPa) (Qty/cv)
WF/PLA	64.5 (8/4.3%)	4.2 (8/8.1%)
WF/aPLA	73.2 (10/6.8%)	4.59 (10/4.6%)
CF/ABS	82.5 (10/11%)	6.95 (10/15%)

Figure 6 shows the flexural stress vs. strain test results for the baseline specimens manufactured using different materials. Different colored curves represent the stress-strain curves for individual specimens. The flexural strength of the 3D-printed CF/ABS was the highest among the three polymer composites, while that of the WF/PLA polymer composite was the lowest. The 3D-printed WF/PLA polymer composites were more ductile, with a strain to failure of 2.7% compared to that of 2.2% of WF/aPLA and 1.6% of CF/ABS. The CF-ABS specimens also showed higher variability in flexural strength and flexural modulus, with a COV of 11% in strength and 15% in flexural modulus.

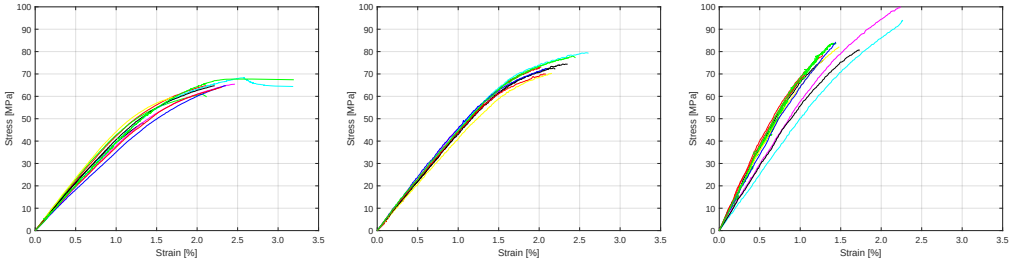

(**a**) WF/PLA (**b**) WF/aPLA (**c**) CF/ABS

Figure 6. Flexural stress vs. strain curves for baseline specimens.

3.3. Flexure Test Results of Specimens Subjected to Accelerated Water Immersion Tests

The WF/PLA specimens failed at a preload of 40 N, indicating severe degradation after 81 days of accelerated water immersion aging. Table 5 presents the average flexural strength and flexural modulus of the WF/aPLA and CF/ABS sets subjected to accelerated water immersion aging. A 73% reduction in flexural strength and a 49% reduction in flexural modulus was observed in WF/aPLA composite specimens. A 49% reduction in flexural strength and an 18% reduction in flexural modulus was observed for CF/ABS composite specimens.

Table 5. Flexural properties of WF/aPLA and CF/ABS after accelerated water immersion aging.

Set	Strength (MPa) (Qty/cv)	Modulus (GPa) (Qty/cv)
WF/aPLA	19.4 (6/4.6%)	2.34 (6/15%)
CF/ABS	42.2 (6/8.9%)	5.74 (6/12%)

Figure 7 shows the stress versus strain plots for the large-format 3D-printed WF/aPLA and CF/ABS specimens subjected to accelerated water immersion aging. Different colored curves represent the stress-strain curves for individual specimens. The flexural strength and flexural moduli of WF/aPLA polymer composite specimens were reduced. The strain to failure was also reduced for WF/aPLA specimens, from an average of 2.2% to an average of 1.3%. Similarly, the flexural strength and flexural moduli of CF/ABS polymer composite specimens were reduced. The strain to failure was also reduced for CF/ABS specimens, from 1.6% to 0.94%.

An ANOVA test was used to compare the flexural strength and modulus between the baseline sets and those under moisture absorption. A p-value < 0.05 was considered statistically significant. Table 6 shows the comparison of the flexural properties before and after the accelerated water immersion aging test. The results of the ANOVA test show that the changes in both flexural strength and flexural moduli were statistically significant for WF/aPLA and CF/ABS polymer composite specimens.

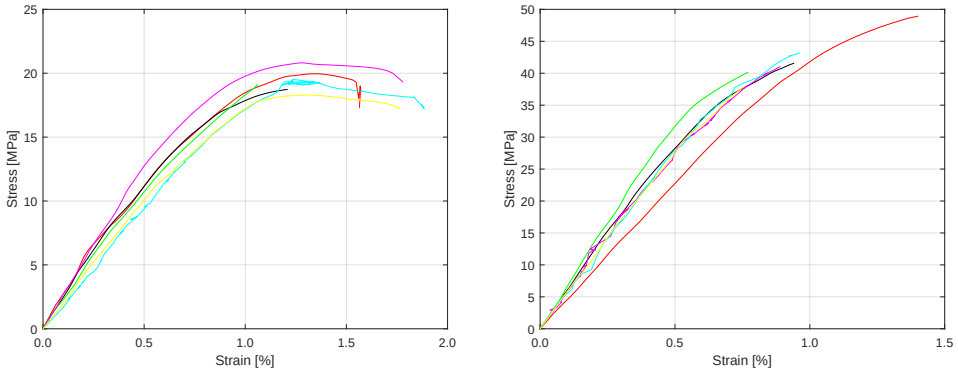

(**a**) WF/aPLA (**b**) CF/ABS

Figure 7. Flexural stress vs. strain curves for specimens subjected to accelerated water immersion.

Table 6. Comparison of flexural properties before and after accelerated water immersion aging.

Set	Baseline	Moisture	% Reduction	*p*-Value
Flexural Strength (MPa)				
WF/aPLA	73.2 (10/6.8%)	19.4 (6/4.7%)	73	1.57×10^{-13}
CF/ABS	82.5 (10/11%)	42.1 (6/8.9%)	49	4.28×10^{-8}
Flexural Modulus (GPa)				
WF/aPLA	4.59 (10/4.6%)	2.34 (6/15%)	49	8.57×10^{-11}
CF/ABS	6.95 (10/15%)	5.74 (6/12%)	18	0.011

Significant reductions in mechanical properties have been reported for ABS as well as PLA composites due to the hygrothermal aging process. Jiang et al. [44] reported a significant reduction in the strength of Jute/PLA composites manufactured using conventional methods due to cracking between the fiber and matrix, associated with the differential swelling and weakening of the interface, and also due to the hydrolysis of the matrix, resulting in microcracking.

Flexural Test Results of Specimens Subjected to Freeze–Thaw Cycling

Table 7 presents the average flexural strength and flexural modulus of the WF/PLA, WF/aPLA, and CF/ABS sets subjected to freeze–thaw cycling.

Table 7. Flexural properties of WF/PLA, WF/aPLA and CF/ABS after freeze–thaw cycling.

Set	Strength (MPa) (Qty/cv)	Modulus (GPa) (Qty/cv)
WF/PLA	64.1 (7/3.8%)	3.64 (7/9.7%)
WF/aPLA	71.9 (10/4.3%)	4.33 (10/4.9%)
CF/ABS	83.9 (6/9.4%)	6.83 (6/16%)

Figure 8 shows the stress versus strain plots for WF/PLA and CF/ABS specimens after freeze–thaw cycling. Different colored curves represent the stress-strain curves for individual specimens. An ANOVA *t*-test, considering a p-value < 0.05 as statistically significant, was used to compare the flexural strength and moduli between the baseline sets and those under moisture absorption. Table 8 shows the p-values obtained for WF/PLA, WF/aPLA, and CF/ABS.

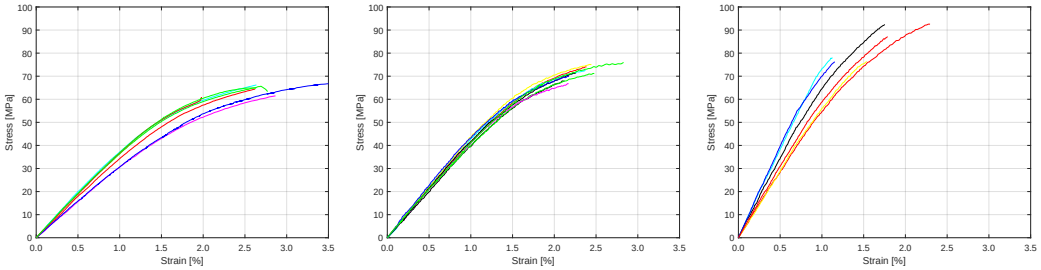

(**a**) WF/PLA (**b**) WF/aPLA (**c**) CF/ABS

Figure 8. Flexural stress vs. strain curves for specimens subjected to freeze–thaw cycling.

Table 8. Comparison of flexural properties before and after freeze–thaw cycling.

Set	Baseline	Freeze–thaw	% Reduction	*p*-Value
Flexural Strength (MPa)				
WF/PLA	64.5 (8/4.3%)	64.1 (7/3.8%)	<1	0.400
WF/aPLA	73.2 (10/6.8%)	71.9 (10/4.3%)	2	0.250
CF/ABS	82.5 (10/11%)	83.9 (6/9.4%)	<1	0.106
Flexural Modulus (GPa)				
WF/PLA	4.21 (8/8.0%)	3.64 (7/9.7%)	14	1.49×10^{-3}
WF/aPLA	4.59 (10/4.6%)	4.33 (10/4.9%)	6	7.22×10^{-3}
CF/ABS	6.95 (10/15%)	6.83 (6/16%)	2	3.36×10^{-1}

Freeze–thaw cycling reduced the flexural moduli of WF/PLA and WF/aPLA, with a statistically significant difference from the baseline set of specimens without freeze–thaw conditioning. For WF/PLA, a reduction of 14% in its flexural modulus of elasticity was observed. For WF/aPLA, a reduction of 6% in its flexural modulus of elasticity was observed. No significant change in the flexural properties of CF/ABS specimens was observed due to freeze–thaw cycling.

Freeze–thaw cycling impacted the bio-based materials, affecting the flexural modulus; in the case of CF/ABS, it did not affect its flexural strength and modulus. Similar results were observed for WPC and ABS materials manufactured using conventional manufacturing methods. Darwish [46] studied the effect of freeze–thaw cycling on desktop-scale 3D-printed CF/ABS composites for 300 cycles and found that there was a loss in tensile strength but an increase in the ductility of the material. However, the reductions in strength were small, and the statistical significance of the change was not analyzed. Pilarski et al. [47,48] studied the effect of freeze–thaw cycles on the strength of wood–plastic composites and found that the change in strength was not significant after two full freeze–thaw cycles but was significant after five freeze–thaw cycles. Consistent with these observations, the change in flexural strength was not found to be statistically significant in this study, where only three freeze–thaw cycles were performed. However, the change in the flexural modulus of large-format 3D-printed composites was found to be statistically significant. Turku et al. [49] also reported that freeze-thaw cycles alone did not affect the mechanical properties. The research also concluded that the loss in properties due to water immersion followed by freeze–thaw cycling was similar to the loss in properties solely due to water immersion. Friedrich et al. [50] mentioned that hygrothermal weather cycles reduced the bonding between the fiber and matrix for swelled and frozen fibers. The freeze–thaw cycling protocol followed in this study adopted only 24 h of water immersion at room temperature before freezing. A longer water immersion period at a higher temperature might allow the fibers to absorb water and undergo swelling and freezing and cause debonding between the fiber and matrix, resulting in reduced mechanical properties. Further investigations are necessary to study the effect of the freeze–thaw cycling of large-format 3D-printed thermoplastic wood–plastic composites at higher moisture content.

4. Conclusions

The durability of the 3D-printed materials was assessed through water absorption and freeze–thaw cycling accelerated testing. The following conclusions have been drawn from the study.

1. Large-format 3D-printed bio-based polymer composite parts absorb significantly more moisture compared to their synthetic counterparts. The bio-based large-format 3D-printed parts were found to have approximately five times the moisture content of the synthetic material. It is noteworthy that the synthetic material approximately reached moisture content equilibrium, while the bio-based materials did not.
2. The coefficients of moisture expansion for the bio-based materials (WF/PLA and WF/aPLA) were orthotropic, with different coefficients of moisture expansion for the three principal material directions.
3. Bio-based 3D-printed parts are more susceptible to moisture degradation, showing a larger reduction in flexural modulus and flexural strength compared to synthetic material parts.
4. Bio-based 3D-printed materials are more susceptible to degradation due to freeze–thaw cycles, showing a significant reduction in the flexural modulus.

Author Contributions: Conceptualization, F.A.S.-R., S.B. and R.A.L.-A.; methodology, F.A.S.-R., S.B. and R.A.L.-A.; software, F.A.S.-R. and S.B.; validation, F.A.S.-R., S.B. and R.A.L.-A.; formal analysis, F.A.S.-R.; investigation, F.A.S.-R., S.B. and R.A.L.-A.; resources, R.A.L.-A.; writing—original draft preparation, F.A.S.-R.; writing—review and editing, S.B. and R.A.L.-A.; visualization, F.A.S.-R. and S.B.; supervision, R.A.L.-A.; project administration, R.A.L.-A.; funding acquisition, R.A.L.-A. All authors have read and agreed to the published version of the manuscript.

Funding: Funding for this research was provided by the Transportation Infrastructure Durability Center at the University of Maine under grant 69A3551847101 from the U.S. Department of Transportation's University Transportation Centers Program, and the Malcolm G. Long '32 Professorship in Civil Engineering.

Institutional Review Board Statement: Not applicable.

Data Availability Statement: The dataset is available on reasonable request from the authors.

Conflicts of Interest: The authors declare no conflicts of interest.

References

1. Shah, J.; Snider, B.; Clarke, T.; Kozutsky, S.; Lacki, M.; Hosseini, A. Large-scale 3D printers for additive manufacturing: Design considerations and challenges. *Int. J. Adv. Manuf. Technol.* **2019**, *104*, 3679–3693. [CrossRef]
2. Bishop, E.G.; Leigh, S.J. Using large-scale additive manufacturing as a bridge manufacturing process in response to shortages in personal protective equipment during the COVID-19 outbreak. *Int. J. Bioprinting* **2020**, *6*, 281.
3. Roschli, A.; Post, B.K.; Chesser, P.C.; Sallas, M.; Love, L.J.; Gaul, K.T. Precast concrete models fabricated with big area additive manufacturing. In Proceedings of the 2018 International Solid Freeform Fabrication Symposium, Austin, TX, USA, 13–15 August 2018.
4. Bhandari, S.; Lopez-Anido, R.; Anderson, J. Large scale 3D printed thermoplastic composite forms for precast concrete structures. In Proceedings of the Conference & Exhibition on Thermoplastic Composites, Bremen, Germany, 13–14 October 2020.
5. Bhandari, S.; Lopez-Anido, R.; Rojas, F.; LeBihan, A. Design and Manufacture of Precast Concrete Formworks Using Polymer Extrusion-Based Large-Scale Additive Manufacturing and Postprocessing. In Proceedings of the ASTM International Conference on Additive Manufacturing (ICAM 2021), Anaheim, CA, USA, 1–5 November 2022; pp. 1–13.
6. Lopez-Anido, R.; Davids, W.; Bhandari, S.; Sheltra, C.A.; Abdel-Magid, B.; Erb, D.F., Jr. Overview of thermoplastic composites in bridge applications. In Proceedings of the European Bridge Conference-2022, Edinburgh, UK, 20–23 June 2022.
7. Peters, B. Additive formwork: 3D printed flexible formwork. In Proceedings of the ACADIA, Los Angles, LA, USA, 23–25 October 2014; Volume 14, pp. 517–522.
8. Bhandari, S.; Lopez-Anido, R.A.; Anderson, J.; Mann, A. Large-scale extrusion-based 3D printing for highway culvert rehabilitation. In Proceedings of the SPE ANTEC, Online, 10–21 May 2021.
9. Ferrini-Mundy, J.; Varahramyan, K. *2022 Research Report: R1 Global Impact-Local Relevance*; Technical Report; University of Maine, Orono, ME, USA, 2023.
10. Liedtka, C. *Life Cycle Analysis and Implications of 3D Printed Bio-Based Homes, A Preliminary Study*; Technical Report; University of Maine, Orono, ME, USA, 2022.

11. Van de Werken, N.; Tekinalp, H.; Khanbolouki, P.; Ozcan, S.; Williams, A.; Tehrani, M. Additively manufactured carbon fiber-reinforced composites: State of the art and perspective. *Addit. Manuf.* **2020**, *31*, 100962. [CrossRef]
12. Zhao, X.; Tekinalp, H.; Meng, X.; Ker, D.; Benson, B.; Pu, Y.; Ragauskas, A.J.; Wang, Y.; Li, K.; Webb, E.; et al. Poplar as biofiber reinforcement in composites for large-scale 3D printing. *ACS Appl. Bio Mater.* **2019**, *2*, 4557–4570. [CrossRef]
13. Lamm, M.E.; Wang, L.; Kishore, V.; Tekinalp, H.; Kunc, V.; Wang, J.; Gardner, D.J.; Ozcan, S. Material extrusion additive manufacturing of wood and lignocellulosic filled composites. *Polymers* **2020**, *12*, 2115. [CrossRef]
14. Talagani, M.; DorMohammadi, S.; Dutton, R.; Godines, C.; Baid, H.; Abdi, F.; Kunc, V.; Compton, B.; Simunovic, S.; Duty, C.; et al. Numerical simulation of big area additive manufacturing (3D printing) of a full size car. *SAMPE J.* **2015**, *51*, 27–36.
15. Karbhari, V.; Chin, J.; Hunston, D.; Benmokrane, B.; Juska, T.; Morgan, R.; Lesko, J.; Sorathia, U.; Reynaud, D. Durability gap analysis for fiber-reinforced polymer composites in civil infrastructure. *J. Compos. Constr.* **2003**, *7*, 238–247. [CrossRef]
16. Gardner, D.J.; Han, Y.; Wang, L. Wood–plastic composite technology. *Curr. For. Rep.* **2015**, *1*, 139–150. [CrossRef]
17. Yu, C.W.; Bull, J.W. *Durability of Materials and Structures in Building and Civil Engineering*; Newcastle University: Newcastle upon Tyne, UK, 2006.
18. Nelson, W.B. *Accelerated Testing: Statistical Models, Test Plans, and Data Analysis*; John Wiley & Sons: Hoboken, NJ, USA, 2009.
19. Stamboulis, A.; Baillie, C.; Garkhail, S.; Van Melick, H.; Peijs, T. Environmental durability of flax fibres and their composites based on polypropylene matrix. *Appl. Compos. Mater.* **2000**, *7*, 273–294. [CrossRef]
20. Stark, N.; Gardner, D. Outdoor durability of wood–polymer composites. In *Wood–Polymer Composites*; Elsevier: Amsterdam, The Netherlands, 2008; pp. 142–165.
21. Gardner, D.J.; Bozo, A. Ten-year field study of wood plastic composites in Santiago, Chile: biological, mechanical and physical property performance. *Maderas. Cienc. Tecnol.* **2018**, *20*, 257–266. [CrossRef]
22. Malpot, A.; Touchard, F.; Bergamo, S. An investigation of the influence of moisture on fatigue damage mechanisms in a woven glass-fibre-reinforced PA66 composite using acoustic emission and infrared thermography. *Compos. Part B Eng.* **2017**, *130*, 11–20. [CrossRef]
23. Pomies, F.; Carlsson, L.A. Analysis of modulus and strength of dry and wet thermoset and thermoplastic composites loaded in transverse tension. *J. Compos. Mater.* **1994**, *28*, 22–35. [CrossRef]
24. Celestine, A.D.N.; Agrawal, V.; Runnels, B. Experimental and numerical investigation into mechanical degradation of polymers. *Compos. Part B Eng.* **2020**, *201*, 108369. [CrossRef]
25. Cormier, D.; Poddar, P. Durability of polymer matrix composites fabricated via additive manufacturing. In *Durability of Composite Systems*; Elsevier: Amsterdam, The Netherlands, 2020; pp. 403–438.
26. Banjo, A.D.; Agrawal, V.; Auad, M.L.; Celestine, A.D.N. Moisture-induced changes in the mechanical behavior of 3D printed polymers. *Compos. Part C Open Access* **2022**, *7*, 100243. [CrossRef]
27. Kakanuru, P.; Pochiraju, K. Moisture ingress and degradation of additively manufactured PLA, ABS and PLA/SiC composite parts. *Addit. Manuf.* **2020**, *36*, 101529. [CrossRef]
28. Xiao, Y.; Zhang, S.; Chen, J.; Guo, B.; Chen, D. Mechanical performance of 3D-printed polyethylene fibers and their durability against degradation. *Materials* **2023**, *16*, 5182. [CrossRef] [PubMed]
29. Dizon, J.R.C.; Gache, C.C.L.; Cascolan, H.M.S.; Cancino, L.T.; Advincula, R.C. Post-processing of 3D-printed polymers. *Technologies* **2021**, *9*, 61. [CrossRef]
30. Afshar, A.; Mihut, D. Enhancing durability of 3D printed polymer structures by metallization. *J. Mater. Sci. Technol.* **2020**, *53*, 185–191. [CrossRef]
31. Głowacki, M.; Skórczewska, K.; Lewandowski, K.; Szewczykowski, P.; Mazurkiewicz, A. Effect of Shock-Variable Environmental Temperature and Humidity Conditions on 3D-Printed Polymers for Tensile Properties. *Polymers* **2023**, *16*, 1. [CrossRef]
32. Grassi, G.; Spagnolo, S.L.; Paoletti, I. Fabrication and durability testing of a 3D printed façade for desert climates. *Addit. Manuf.* **2019**, *28*, 439–444. [CrossRef]
33. Duty, C.E.; Kunc, V.; Compton, B.; Post, B.; Erdman, D.; Smith, R.; Lind, R.; Lloyd, P.; Love, L. Structure and mechanical behavior of Big Area Additive Manufacturing (BAAM) materials. *Rapid Prototyp. J.* **2017**, *23*, 181–189. [CrossRef]
34. Somireddy, M.; Czekanski, A. Anisotropic material behavior of 3D printed composite structures–Material extrusion additive manufacturing. *Mater. Des.* **2020**, *195*, 108953. [CrossRef]
35. Zou, R.; Xia, Y.; Liu, S.; Hu, P.; Hou, W.; Hu, Q.; Shan, C. Isotropic and anisotropic elasticity and yielding of 3D printed material. *Compos. Part B Eng.* **2016**, *99*, 506–513. [CrossRef]
36. *ASTM D5229*; Standard Test Method for Moisture Absorption Properties and Equilibrium Conditioning of Polymer Matrix Composite Materials. ASTM International: West Conshohocken, PA, USA, 2020.
37. Pönninger, A.; Defoort, B. Determination of the coefficient of moisture expansion (CME). In *Materials in a Space Environment*; ESA Publications: Noordwijk, The Netherlands, 2003; Volume 540, pp. 567–572.
38. Chaid, J.S.; Abdallah, F.A.; Jalil, I.M. Calculation of moisture expansion coefficient of the above knee prosthetic socket lamination materials. *J. Eng. Sustain. Dev.* **2016**, *20*, 189–196.
39. *ASTM D7992*; Standard Practice for Freeze/Thaw Conditioning of Pultruded Fiber Reinforced Polymer (FRP) Composites Used in Structural Designs. ASTM International: West Conshohocken, PA, USA, 2015.
40. *ASTM D7264*; Standard Test Method for Flexural Properties of Polymer Matrix Composite Materials. ASTM International: West Conshohocken, PA, USA, 2007.

41. Wang, W.; Morrell, J.J. Water sorption characteristics of two wood-plastic composites. *For. Prod. J.* **2004**, *54*, 12.
42. Kim, J.W.; Harper, D.P.; Taylor, A.M. Effect of wood species on water sorption and durability of wood-plastic composites. *Wood Fiber Sci.* **2008**, *40*, 519–531.
43. Huang, S.H.; Cortes, P.; Cantwell, W. The influence of moisture on the mechanical properties of wood polymer composites. *J. Mater. Sci.* **2006**, *41*, 5386–5390. [CrossRef]
44. Jiang, N.; Yu, T.; Li, Y.; Pirzada, T.J.; Marrow, T.J. Hygrothermal aging and structural damage of a jute/poly (lactic acid)(PLA) composite observed by X-ray tomography. *Compos. Sci. Technol.* **2019**, *173*, 15–23. [CrossRef]
45. Aniskevich, A.; Bulderberga, O.; Stankevics, L. Moisture Sorption and Degradation of Polymer Filaments Used in 3D Printing. *Polymers* **2023**, *15*, 2600. [CrossRef]
46. Darwish, O.M. Effect of Saline Immersion and Freeze-Thaw Cycles on Performance of Fused Deposition Modelling (FDM) Materials. Ph.D. Thesis, University of Dayton, Dayton, OH, USA, 2019.
47. Pilarski, J.M.; Matuana, L.M. Durability of wood flour-plastic composites exposed to accelerated freeze–thaw cycling. II. High density polyethylene matrix. *J. Appl. Polym. Sci.* **2006**, *100*, 35–39. [CrossRef]
48. Pilarski, J.M.; Matuana, L.M. Durability of wood flour-plastic composites exposed to accelerated freeze–thaw cycling. Part I. Rigid PVC matrix. *J. Vinyl Addit. Technol.* **2005**, *11*, 1–8. [CrossRef]
49. Turku, I.; Kärki, T.; Puurtinen, A. Durability of wood plastic composites manufactured from recycled plastic. *Heliyon* **2018**, *4*, e00559. [CrossRef] [PubMed]
50. Friedrich, D.; Luible, A. Investigations on ageing of wood-plastic composites for outdoor applications: A meta-analysis using empiric data derived from diverse weathering trials. *Constr. Build. Mater.* **2016**, *124*, 1142–1152. [CrossRef]